

See discussions, stats, and author profiles for this publication at: <https://www.researchgate.net/publication/257887818>

# Triazole–Dithiocarbamate Based Selective Lysine Specific Demethylase 1 (LSD1) Inactivators Inhibit Gastric Cancer Cell Growth, Invasion, and Migration

ARTICLE in JOURNAL OF MEDICINAL CHEMISTRY · OCTOBER 2013

Impact Factor: 5.45 · DOI: 10.1021/jm401002r · Source: PubMed

CITATIONS

22

READS

70

16 AUTHORS, INCLUDING:



Yingchao Duan

Xin Xiang Medical University

8 PUBLICATIONS 101 CITATIONS

SEE PROFILE



David L Mobley

University of California, Irvine

55 PUBLICATIONS 2,779 CITATIONS

SEE PROFILE



Yanyan Zhu

Zhengzhou University

55 PUBLICATIONS 610 CITATIONS

SEE PROFILE



Hong-Min Liu

Zhengzhou University

174 PUBLICATIONS 1,454 CITATIONS

SEE PROFILE

# Triazole–Dithiocarbamate Based Selective Lysine Specific Demethylase 1 (LSD1) Inactivators Inhibit Gastric Cancer Cell Growth, Invasion, and Migration

Yi-Chao Zheng,<sup>†,‡,§</sup> Ying-Chao Duan,<sup>†,‡,§</sup> Jin-Lian Ma,<sup>†,‡</sup> Rui-Min Xu,<sup>†,‡</sup> Xiaolin Zi,<sup>||</sup> Wen-Lei Lv,<sup>†,‡</sup> Meng-Meng Wang,<sup>†,‡</sup> Xian-Wei Ye,<sup>†,‡</sup> Shun Zhu,<sup>⊥</sup> David Mobley,<sup>⊥</sup> Yan-Yan Zhu,<sup>§</sup> Jun-Wei Wang,<sup>†,‡</sup> Jin-Feng Li,<sup>†,‡</sup> Zhi-Ru Wang,<sup>†,‡</sup> Wen Zhao,<sup>†,‡</sup> and Hong-Min Liu\*,<sup>†,‡</sup>

<sup>†</sup>School of Pharmaceutical Sciences, Zhengzhou University, 100 Kexue Avenue, Zhengzhou, Henan 450001, China

<sup>‡</sup>New Drug Research and Development Center, Zhengzhou University, 100 Kexue Avenue, Zhengzhou, Henan 450001, China

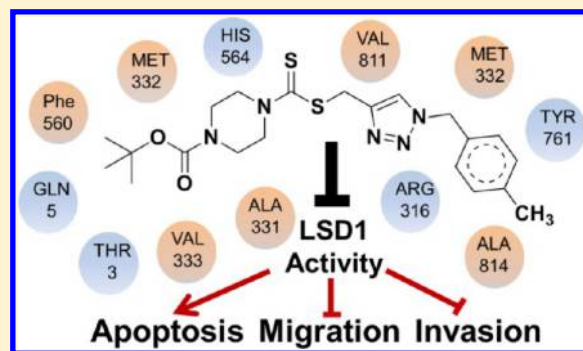
<sup>§</sup>The College of Chemistry and Molecular Engineering, Zhengzhou University, 100 Kexue Avenue, Zhengzhou, Henan 450001, China

<sup>||</sup>Department of Urology, School of Medicine, University of California, Irvine, Orange, California 92688, United States

<sup>⊥</sup>Department of Pharmaceutical Sciences, University of California, Irvine, California 92697, United States

## S Supporting Information

**ABSTRACT:** Lysine specific demethylase 1 (LSD1), the first identified histone demethylase, plays an important role in epigenetic regulation of gene activation and repression. The up-regulated LSD1's expression has been reported in several malignant tumors. In the current study, we designed and synthesized five series of 1,2,3-triazole–dithiocarbamate hybrids and screened their inhibitory activity toward LSD1. We found that some of these compounds, especially compound **26**, exhibited the most specific and robust inhibition of LSD1. Interestingly, compound **26** also showed potent and selective cytotoxicity against LSD1 overexpressing gastric cancer cell lines MGC-803 and HGC-27, as well as marked inhibition of cell migration and invasion, compared to 2-PCPA. Furthermore, compound **26** effectively reduced the tumor growth bared by human gastric cancer cells in vivo with no signs of adverse side effects. These findings suggested that compound **26** deserves further investigation as a lead compound in the treatment of LSD1 overexpressing gastric cancer.



## INTRODUCTION

Epigenetic post-transcriptional modifications on histone, including acetylation, methylation, and phosphorylation, modulate gene activation and repression. Among these modifications, methylation and demethylation of lysine are dynamically regulated by a number of histone lysine methyltransferases (HKMTs) and histone lysine demethylases (HKDMs) including lysine specific demethylase 1 (LSD1). LSD1, the first characterized demethylase in 2004,<sup>1</sup> is a highly conserved flavin adenine dinucleotide (FAD) dependent oxidative enzyme containing amine oxidase domain. It demethylates mono- and dimethylated K4 and K9 of histone 3, as well as p53, E2F transcription factor 1 (E2F1), and DNA methyltransferases (DNMTs) and further regulates their downstream cellular function.<sup>2–7</sup> LSD1 has been reported to be overexpressed in many malignant tumors, including breast, colon, prostate, lung, gastric cancers, and others.<sup>8–16</sup> Down-regulation of LSD1 by RNAi or various kinds of inhibitors has been shown to effectively treat those cancers by inducing re-expression of aberrantly silenced genes.<sup>11,12,17–23</sup> Therefore,

LSD1 has been considered an important and promising anticancer target.

As a member of monoamine oxidase (MAO) family, LSD1 utilizes a noncovalently bound FAD as its cofactor to oxidatively remove the methyl groups of its substrates.<sup>1</sup> MAO-A and MAO-B, another two members of MAO family, share the same mechanism and cofactor of LSD1 in the cleavage of the inactivated carbon–nitrogen bonds from their substrates.<sup>24</sup> MAO inactivators (Figure 1), such as pargyline (**1**), phenelzine (**2**), and tranylcypromine (**3**, 2-PCPA), have been reported to function as nonselective LSD1 inhibitors.<sup>25</sup> In

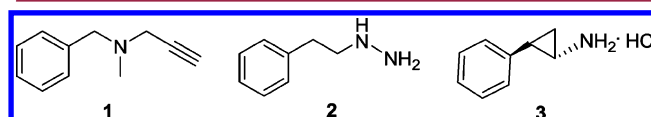
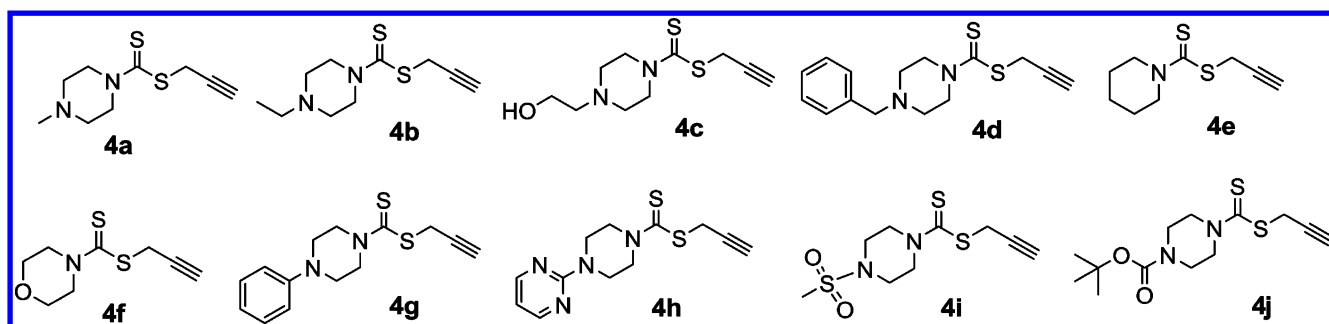
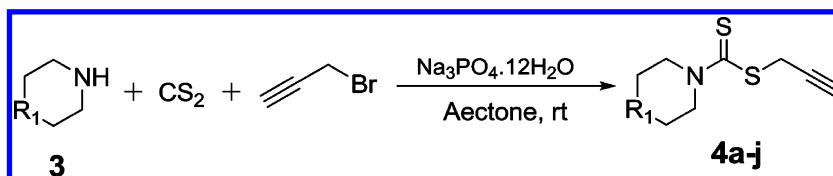
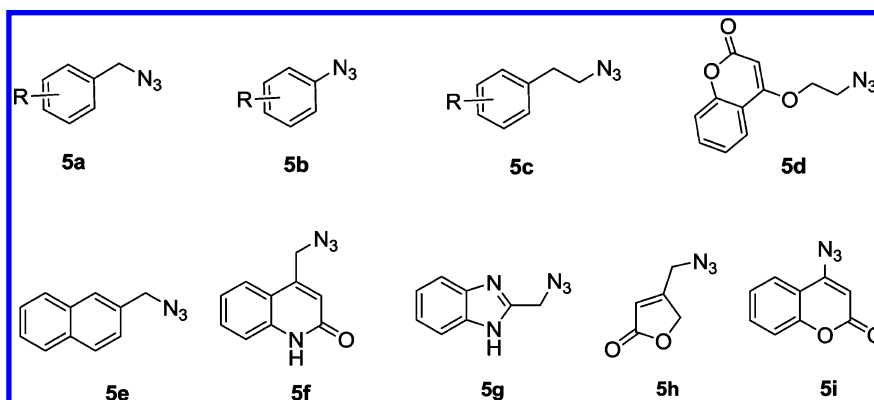


Figure 1. MAO inhibitors that inhibit LSD1.

Received: July 3, 2013

Published: October 16, 2013

Scheme 1. Synthesis of Alkyne Intermediates

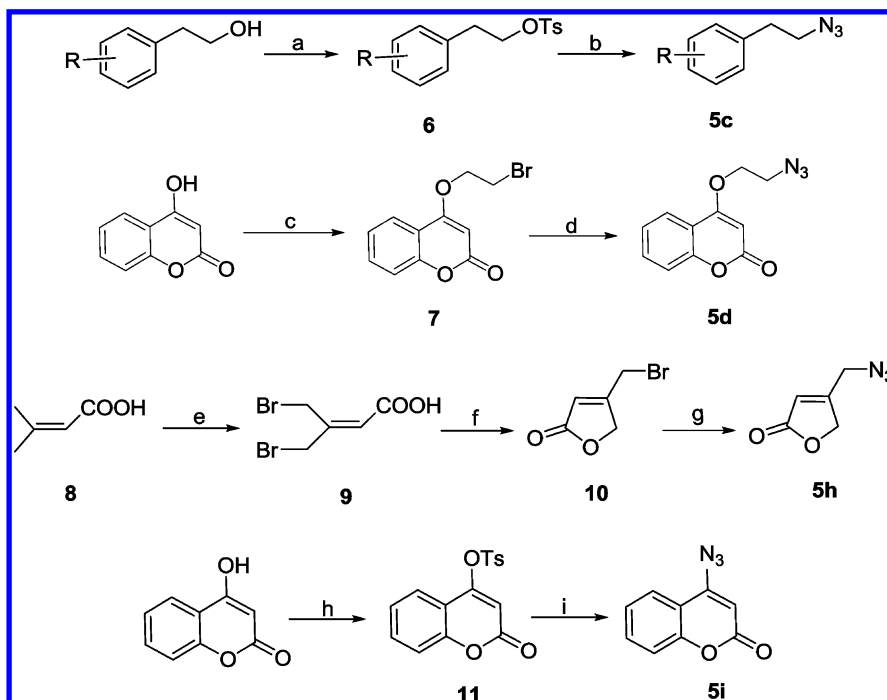
Figure 2. Alkyne intermediates **4a-j** used in the present study.Figure 3. Azides **5a-i** used in the present study.

addition, 2-PCPA derivatives, peptides, and polyamine analogues have been synthesized as LSD1 inhibitors.<sup>12,17,18,26–33</sup> However, only three new classes of LSD1 chemical inhibitors, including amidoxime based compounds,<sup>22</sup> amidinoguanidinium compounds,<sup>34</sup> and phenyloxazoles,<sup>19</sup> have been reported during the past 2 years. Highly selective LSD1 inhibitors with strong toxicity toward cancer cells and less or no side effects on normal cells remain to be identified.

The azole heterocycles (pyrazole, including thiazole, imidazole, pyrrole, oxadiazole, and triazole) have attracted more attention from medicinal chemists for many years because of their numerous biological activities,<sup>35,36</sup> especially their MAO inhibitory effect.<sup>37–43</sup> Among these azole heterocycles, 1,2,3-triazole was mainly used based on its synthetic accessibility by click chemistry as well as its capacity for binding of biomolecular targets. Recently, several inhibitors toward MAO-A were developed accordingly.<sup>44,45</sup> Furthermore, click chemistry has been widely used for synthesizing other inhibitors against epigenetic enzymes, such as HDAC.<sup>46,47</sup> Hence, in this study, 1,2,3-triazole was chosen as a part of our target compound skeleton.

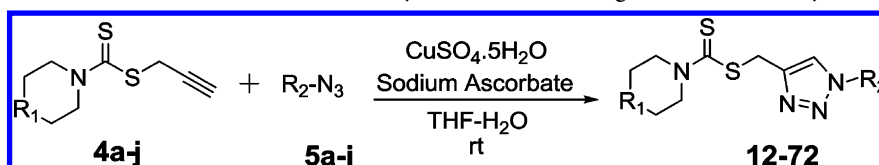
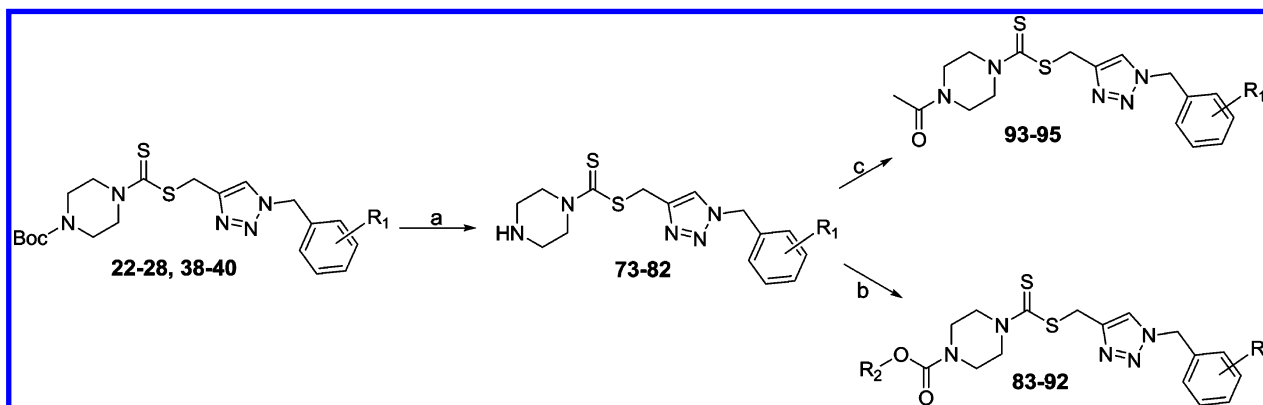
Dithiocarbamates were selected because of their inhibitory activities against fungal, bacteria, and malignant cancer.<sup>48–50</sup> Disulfiram (DSF), as a supporting treatment of chronic alcoholism, is commercially available, and recently it has been

reported as P-glycoprotein efflux pump modulator with antifungal potential.<sup>51</sup> Furthermore, when disulfiram creates complexes with metals, it becomes a proteasome inhibitor and acts as a promising approach for anticancer therapy.<sup>51</sup> BO-3482, a novel dithiocarbamate-containing carbapenem with activity against MRSA (methicillin-resistant *Staphylococcus aureus*), has been tested in preclinical trial.<sup>52,53</sup> Meanwhile, we have previously reported a pool of novel butenolides-containing dithiocarbamates with good anticancer activity.<sup>54</sup> Therefore, on the basis of an existing pool of triazole-containing dithiocarbamates,<sup>55</sup> a library with 84 1,2,3-triazole–dithiocarbamate hybrids was synthesized by the click chemistry approach. Their anti-LSD1 activity and cytotoxicities were then determined. We found that compared to 2-PCPA, a nonselective LSD1 inhibitor, triazole–dithiocarbamate based LSD1 inhibitors, especially compound **26**, are more potent and exhibit selective inhibition of the growth of LSD1 overexpressing gastric cancer cell lines. Compound **26** also impaired cell migration and invasion and significantly inhibited tumor growth in vivo. These findings indicate that triazole–dithiocarbamate based LSD1 inhibitors represent a novel class of LSD1 inhibitors against LSD1 overexpressing gastric cancer.

Scheme 2. Synthesis of the Azides 5c, 5d, 5h, and 5i<sup>a</sup>

<sup>a</sup>Reagents and conditions: (a) TsCl, Et<sub>3</sub>N, DMAP, CH<sub>2</sub>Cl<sub>2</sub>, rt; (b) NaN<sub>3</sub>, CH<sub>3</sub>CN, reflux; (c) 1,2-dibromoethane, K<sub>2</sub>CO<sub>3</sub>, CH<sub>3</sub>CN, reflux; (d) NaN<sub>3</sub>, acetone–H<sub>2</sub>O (4:1), reflux; (e) NBS, Ph(CO)<sub>2</sub>O<sub>2</sub>, CCl<sub>4</sub>, reflux; (f) 5% aq NaOH, rt, 12 h; (g) NaN<sub>3</sub>, acetone–H<sub>2</sub>O (4:1), rt; (h) TsCl, Et<sub>3</sub>N, CH<sub>2</sub>Cl<sub>2</sub>, rt; (i) NaN<sub>3</sub>, DMF, 80 °C.

Scheme 3. Synthesis of 1,2,3-Triazole–Dithiocarbamate Hybrids 12–72 through Click Chemistry

Scheme 4. Synthesis of 1,2,3-Triazole–Dithiocarbamate Hybrids 73–96<sup>a</sup>

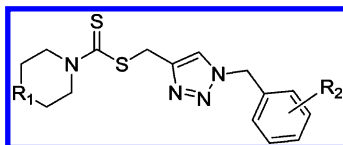
<sup>a</sup>Reagents and conditions: (a) CF<sub>3</sub>COOH, CH<sub>2</sub>Cl<sub>2</sub>, 0 °C to rt; (b) R<sub>2</sub>OCOCl, K<sub>2</sub>CO<sub>3</sub>, CH<sub>2</sub>Cl<sub>2</sub>, rt; (c) CH<sub>3</sub>COCl, Et<sub>3</sub>N, CH<sub>2</sub>Cl<sub>2</sub>, rt.

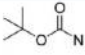
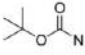
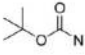
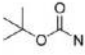
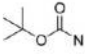
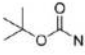
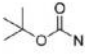
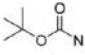
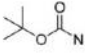
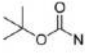
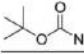
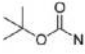
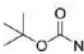
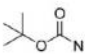
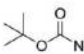
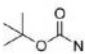
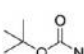
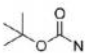
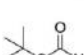
## CHEMISTRY

Alkyne intermediates **4a–j** were synthesized as shown in Scheme 1. Commercially available amines were treated with CS<sub>2</sub> and propargyl bromide in the presence of Na<sub>3</sub>PO<sub>4</sub>·12H<sub>2</sub>O in one pot to provide **4a–j** (Figure 2).

Azides **5a** and **5e–g** (Figure 3) were obtained from commercially available bromides by direct azide displacement. Azide **5b** was prepared using classical diazotation–azidation

protocols.<sup>56</sup> The synthesis of azide intermediates **5c**, **5d**, **5h**, and **5i** (Figure 3) is shown in Scheme 2. Substituted phenethyl alcohol was esterified to tosylate **6**, which was converted to azide derivative **5c** by reacting with sodium azide in acetonitrile. Hydroxycoumarin was treated with 1,2-dibromoethane or tosyl chloride and then with sodium azide to acquire **5d** and **5i**, respectively. Azide derivative **5h** was prepared by a sodium

Table 1. Structures of Compounds 12–40 and Their Inhibition Rates ( $IC_{50}$ ) to the Purified LSD1 Recombinant in Vitro

Comp.	R <sub>1</sub>	R <sub>2</sub>	IC <sub>50</sub> (μM)	Comp.	R <sub>1</sub>	R <sub>2</sub>	IC <sub>50</sub> (μM)
12	CH <sub>2</sub>	<i>o</i> -F	>125	27		<i>p</i> -OCH <sub>3</sub>	18.4±2.5
13	CH <sub>2</sub>	<i>p</i> -F	>125	28		<i>m</i> -CH <sub>3</sub>	43.3±5.9
14	CH <sub>2</sub>	<i>p</i> -CH <sub>3</sub>	>125	29		<i>o</i> -CH <sub>3</sub>	>125
15	CH <sub>2</sub>	H	>125	30		<i>p</i> -CF <sub>3</sub>	>125
16	CH <sub>2</sub>	<i>p</i> -Cl	>125	31		<i>o</i> -CF <sub>3</sub>	>125
17	0	H	>125	32		<i>o</i> -Br	27.5±3.7
18	0	<i>o</i> -F	>125	33		<i>p</i> -OH	70.7±1.2
19	0	<i>p</i> -F	>125	34		<i>o</i> -OH	69.2±3.6
20	0	<i>p</i> -CH <sub>3</sub>	>125	35		<i>p</i> -NO <sub>2</sub>	>125
21	0	<i>p</i> -Cl	>125	36		<i>m</i> -OH	77.1±3.1
22		<i>o</i> -F	<b>8.0±1.0</b>	37		<i>o, p</i> -diOH	81.3±2.0
23		<i>p</i> -F	21.6±2.3	38		<i>m, p</i> -diCl	88.9±3.2
24		<i>o</i> -Cl	11.5±2.1	39		<i>o, o</i> -diF	51.2±4.3
25		<i>p</i> -Cl	56.5±2.8	40		<i>m, p, m</i> -triOCH <sub>3</sub>	19.0±2.5
26		<i>p</i> -CH <sub>3</sub>	<b>2.1±0.7</b>	2-PCPA	-	-	27.8±2.6

azide substitution of **10**, obtained from starting material **8** from the reported procedures.<sup>57,58</sup>

The 1,2,3-triazole–dithiocarbamate hybrids **12–72** were synthesized through a Huisgen 1,3-dipolar cycloaddition between alkynes **4a–j** and azides **5a–i** using copper sulfate and sodium ascorbate in aqueous THF (Scheme 3). The synthesis of 1,2,3-triazole–dithiocarbamate hybrids **73–95** is shown in Scheme 4. **22–28** and **38–40** were deprotected using trifluoroacetic acid in dichloromethane to afford compounds **73–82**. Compounds **83–92** were obtained by reaction of **73–78**, **81**, and **82** with corresponding chloroformic ester under basic condition. Compounds **73–75** and **77** were treated with acetyl chloride and Et<sub>3</sub>N to obtain **93–95**.

## RESULTS AND DISCUSSION

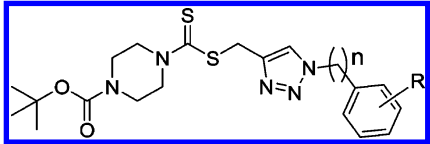
**Identification of LSD1 Inhibitors and Structure–Activity Relationship (SAR) Studies.** To determine the inhibitory activity of this compound library against LSD1, we generated a LSD1 recombinant expressing vector containing human LSD1 cDNA. The expression of recombinant LSD1 was then induced in *Escherichia coli* (*E. coli*) and purified as published.<sup>18</sup> The demethylation activity of the recombinant LSD1 was further determined by a fluorescence-based method, using synthesized H3K4me2 as a substrate.<sup>32</sup> All the compounds synthesized in this study were examined in vitro for their inhibitory effect on LSD1 activity. 2-PCPA was chosen as a positive control. The results are summarized as Tables 1–5.



The in vitro inhibitory activity results of compounds 12–40 against LSD1 were determined initially and shown in Table 1. With the exception of compounds 29–31 and 36, all the compounds bearing a carbamate moiety exhibit moderate to good potency with  $IC_{50}$  values ranging from 2.1 to 88.9  $\mu M$ . Among them, compound 26 shows the most potent activity to LSD1, with an  $IC_{50}$  of 2.1  $\mu M$ , which is 14 times higher than that of 2-PCPA. Moreover, compounds 22–24, 27, and 40 are more potent than 2-PCPA, with  $IC_{50}$  values in the single- or double-digit micromolar range. During the SAR studies, we found that the substitution on the phenyl ring was important for the in vitro LSD1 inhibitory activity showing over 35-fold activity loss, when the methyl group was replaced with the hydroxyl group (compound 26 vs 33). We also observed that the para substitution was preferential: the *p*-CH<sub>3</sub> derivative compound 26 was more potent against LSD1 than the *m*-CH<sub>3</sub> derivative 28 ( $IC_{50}$  = 43.3  $\mu M$ ) and the *o*-CH<sub>3</sub> derivative 29 without any detectable activity. The nitrogen of the piperidine was essential. When the nitrogen was replaced with a methylene or an oxygen atom (12–16, 17–21), their inhibitory activities to LSD1 were completely lost.

To determine whether the length of carbon tether between the triazole ring and the benzene ring might affect the compounds' binding of LSD1, compounds 41–46 were synthesized and their LSD1 inhibitory activities were shown in Table 2. With either extension or reduction of the carbon

Table 2. Effect of Linker Length on LSD1 Inhibition



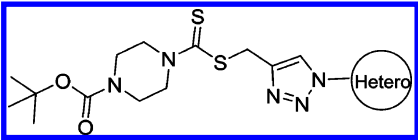
compd	n	R	$IC_{50}$ ( $\mu M$ )
41	0	<i>p</i> -CH <sub>3</sub>	>125
42	0	<i>p</i> -OCH <sub>3</sub>	>125
43	0	<i>o</i> -F	>125
44	0	<i>m</i> -CF <sub>3</sub>	>125
45	2	<i>p</i> -CH <sub>3</sub>	>125
46	2	<i>p</i> -F	>125

tether length by one carbon, a complete loss of potency was observed. Those results suggested that the linker between the benzene ring and the triazole plays an important role in their activities.

The importance of the benzene ring in the LSD1 inhibitory activity was also explored (Table 3). Replacing the phenyl scaffold of compound 26 with coumarin ring (47), naphthalene ring (48), quinolinone ring (49), benzoxazole ring (50), or butenolide ring (51) led to a complete loss of activity or very weak binding affinity, indicating the significance of the benzene ring in retaining their activity.

Furthermore, the importance of substituents on the N-atom (Table 4) was investigated. Changing the *tert*-butoxycarbonyl group to alkyl chain methyl, ethyl, benzyl, or hydroxyethyl resulted in inactive compounds 53–63. Replacing the *tert*-butoxycarbonyl group by phenyl (as in 64–66), 2-pyrimidinyl (as in 67 and 68), or mesyl (as in 69–71) caused dramatic loss of activity. Removing the *tert*-butoxycarbonyl group was clearly detrimental for the inhibition of LSD1, such as compound 26 (2.1  $\mu M$ ) compared to 77 (28.9  $\mu M$ ) and 73 (17.3  $\mu M$ ). These modifications and SAR studies revealed that

Table 3. Effect of Different Aromatic Rings on LSD1 Inhibition



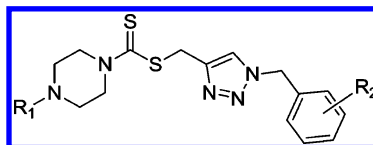
Comp.	Hetero	$IC_{50}$ ( $\mu M$ )
47		>125
48		>125
49		>125
50		>125
51		>125
52		>125

the *tert*-butoxycarbonyl group is critical for their inhibitory activity.

We next synthesized compounds 83–95 to explore the bulk of carbamate moiety and the effect of the oxygen atom. The results were shown in Table 5. Changing the *tert*-butyl carbamates to benzyl carbamates (83–90) dramatically decreased the inhibitory activity, by comparing 87 and 88 with 26 and 27. Compared to compound 26, the ethyl carbamate 91 and isopropyl carbamate 92 showed 8.5- to 7.5-fold loss of activity in their  $IC_{50}$  values, respectively. This finding indicated that steric hindrance of the carbamoyl moiety was of pivotal importance in their activity. The role of the oxygen atom was investigated by preparing compounds 93–95, in which the oxygen atom was replaced with a methylene group. These compounds showed moderate activity with  $IC_{50}$  ranging from 25.3 to 47.1  $\mu M$ , which is consistent with the results described above that the *tert*-butoxycarbonyl group is critical for the inhibitory activity.

**In Vitro Inhibition Properties of Compound 26 to the Recombinant LSD1 and Its Homologies: LSD2, MAO-A, and MAO-B.** Having identified compound 26 as a highly potent LSD1 inhibitor, we further determined the dissociation constant ( $K_d$ ) of compound 26 by microscale thermophoresis (MST) experiment. The  $K_d$  values for compound 26 and 2-PCPA were 0.35 and 46.3  $\mu M$  (Figure 4A,B), respectively, indicating the robust binding affinity of compound 26 to LSD1 compared to 2-PCPA (Figure 4A,B). Then the inhibitory properties of compound 26 were characterized. We found that during 60 min, the inhibition of compound 26 to LSD1 activity with three different concentrations (0.5, 2.5, and 12.5  $\mu M$ ) is time independent (Figure 4D). To test the reversibility of compound 26 for LSD1, a dilution assay was used. Our analysis

Table 4. Effect of Different Substituents at the N-Atom on LSD1 Inhibition

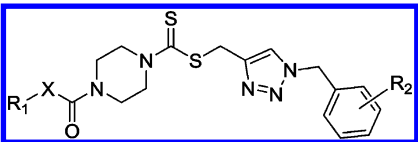


Comp.	R <sub>1</sub>	R <sub>2</sub>	IC <sub>50</sub> (μM)	Comp.	R <sub>1</sub>	R <sub>2</sub>	IC <sub>50</sub> (μM)
53	CH <sub>3</sub>	<i>o</i> -F	>125	68		<i>o</i> -F	39.8±1.1
54	CH <sub>3</sub>	<i>p</i> -CH <sub>3</sub>	>125	69		<i>p</i> -F	43.9±2.5
55	CH <sub>3</sub>	<i>p</i> -F	>125	70		<i>p</i> -CH <sub>3</sub>	35.7±2.0
56	CH <sub>3</sub>	<i>o</i> -Cl	>125	71		<i>o</i> -F	45.7±1.9
57		<i>p</i> -CH <sub>3</sub>	>125	72		<i>p</i> -F	55.1±3.3
58		<i>o</i> -F	>125	73	H	<i>o</i> -F	17.3±1.7
59		<i>p</i> -CH <sub>3</sub>	>125	74	H	<i>p</i> -F	69.3±1.8
60		<i>o</i> -F	>125	75	H	<i>o</i> -Cl	>125
61		<i>p</i> -CH <sub>3</sub>	83.4±2.1	76	H	<i>p</i> -Cl	>125
62		<i>o</i> -F	100.1±9.3	77	H	<i>p</i> -CH <sub>3</sub>	28.9±2.0
63		<i>p</i> -F	>125	78	H	<i>p</i> -OCH <sub>3</sub>	19.5±1.9
64		<i>p</i> -CH <sub>3</sub>	40.3±2.1	79	H	<i>p</i> -CF <sub>3</sub>	87.4±2.3
65		<i>o</i> -F	>125	80	H	<i>o, o</i> -diF	>125
66		<i>p</i> -F	>125	81	H	<i>m, p</i> -diCl	>125
67		<i>p</i> -CH <sub>3</sub>	27.6±1.2	82	H	<i>m, p, m</i> -triOCH <sub>3</sub>	>125

suggested that dilution of the LSD1/compound **26** mixture by 80-fold resulted in the recovery of LSD1 activity, which means the molecule may interact noncovalently with the enzyme. However, in the presence of the covalently binding inhibitor 2-PCPA, LSD1 activity cannot be recovered after dilution (Figure 4E). These results indicate the reversibility of compound **26**, compared to 2-PCPA. Dialysis experiment was also performed against hepes buffer after LSD1 was inactivated by a high concentration of compound **26**. After the dialysis, the activity can be restored (Figure 4F), which further supports the reversible inhibitory of compound **26**. Next, the competitive analysis was performed to test the hypothesized binding sites of compound **26** on LSD1. With classic Lineweaver–Burk plots,<sup>59</sup> we characterized that compound **26** was a noncompetitive inhibitor over LSD1 substrate, H3K4me2 (Figure 4G), but a competitive inhibitor over LSD1 cofactor FAD (Figure 4H).

These results indicate that compound **26** may penetrate into the cavity in LSD1 where FAD stands and reduce the recombinant activity. Another dialysis experiment was done to verify the FAD ejection with compound **26** treatment on LSD1. The inhibitor, FAD and LSD1 were incubated and dialyzed against the hepes buffer containing the same concentration of inhibitor. Then the amount of FAD in the dialysis tubes was monitored at 468 nm with a UV/vis spectrophotometer. After dialysis, the amount of FAD in the compound **26** dialysis tube was much less than that in control group (data not shown), indicating that the FAD may be ejected with the treatment of compound **26**. The  $K_d$  value of FAD is 0.182 μM (Figure 4C), smaller than that of compound **26**, indicating that FAD, as the cofactor of LSD1, binds to this enzyme more tightly than compound **26**. However, at a relative higher concentration, compound **26** may still exhibit

Table 5. Effect of the Bulk of Carbamate Moiety on LSD1 Inhibition



Comp.	R <sub>1</sub>	R <sub>2</sub>	X	IC <sub>50</sub> (μM)
83		<i>o</i> -F	O	32.8±2.0
84		<i>p</i> -F	O	47.6±4.3
85		<i>o</i> -Cl	O	53.2±2.9
86		<i>p</i> -Cl	O	>125
87		<i>p</i> -CH <sub>3</sub>	O	22.4±1.0
88		<i>p</i> -OCH <sub>3</sub>	O	35.1±2.1
89		<i>m, p</i> -diCl	O	29.5±1.3
90		<i>m, p, m</i> -triOCH <sub>3</sub>	O	43.5±4.1
91		<i>p</i> -CH <sub>3</sub>	O	17.0±1.2
92		<i>p</i> -CH <sub>3</sub>	O	15.0±0.7
93	H	<i>o</i> -F	CH <sub>2</sub>	30.2±1.9
94	H	<i>p</i> -F	CH <sub>2</sub>	47.1±2.0
95	H	<i>p</i> -CH <sub>3</sub>	CH <sub>2</sub>	25.3±2.2

competitive inhibition against FAD. It is not so common to create a FAD competitor. But there are some published examples on FAD competitors. Quinine and mepacrine (atabrine) were stated to inhibit D-amino acid oxidase by competing with FAD.<sup>60</sup> Chlorpromazine (CPZ), a dopamine D2 receptor antagonist introduced in the treatment of schizophrenia in the early 1950s, acts as a FAD-competitive inhibitor of human D-amino acid oxidase (hDAAO) with similar structure.<sup>61</sup> K001, which competes for FAD binding, inhibits cryptochrome (CRY) ubiquitylation and lengthens the circadian cycle.<sup>62</sup> There are some other papers published on FAD ejectors.<sup>63,64</sup> EN460, an inhibitor of endoplasmic reticulum oxidation 1 (ERO1), was reported in 2010.<sup>64</sup> This compound exhibits selectivity for ERO1 and displaces bound FAD from the active site of the enzyme. Nevertheless, the structure of EN460 is different from that of FAD. Furthermore, several other compounds were obtained with virtual screening for a lead, which would compete with FAD.<sup>63</sup> Hence, although the structure of compound **26** is not similar to that of FAD, it is still possibly for it to act as FAD competitor or FAD ejector. On the other hand, compound **26** may also bind to an allosteric

site of LSD1,<sup>65–67</sup> resulting in an apparent change in binding affinity of another ligand at a distinctly different site. Furthermore docking analysis illustrated the interaction between compound **26** and LSD1.

Activity of LSD1 and LSD2 recombinant was evaluated by quantifying the demethylase byproduct H<sub>2</sub>O<sub>2</sub> with Amplex Red method coupled with HRP. Activity of MAO-A and MAO-B was evaluated by the commercialized kit. Data are the mean ± SD. All experiments were repeated at least three times.

As LSD1 belongs to the monoamine oxidase (MAO) family, the inhibitory effects of compounds **22** and **26** to its homologues MAO-A and MAO-B were also examined using commercially available kits. Compared to 2-PCPA, compounds **22** and **26** had no significant effects on MAO-A and MAO-B activities (Table 6). Recently, another FAD dependent lysine demethylase, named LSD2, was identified with 45% sequence identity with LSD1.<sup>68,69</sup> Therefore, the LSD2 recombinant encoding 22-822AA was also generated from *E. coli*, and the purified recombinant was then applied to its activity assay. As shown in Table 2, compounds **22** and **26** showed poor inhibitory effect against LSD2 recombinant. These findings indicated the high selectivity of this class of inhibitors on LSD1 *in vitro*.

#### Docking and Molecular Dynamics (MD) Simulations.

Predictions of the binding modes involve a comprehensive evaluation of the center structures of the clusters generated from a Perron-cluster cluster analysis (PCCA) using the following three criteria: (1) the protein–ligand interaction energy obtained from the PCCA analysis; (2) the number of hydrogen bonds between the protein and the ligand calculated using a distance (donor–acceptor) and angle cutoff of 3 Å and 20°, respectively; (3) the stability of the ligand in the binding site during MD simulations. By use of the above procedure, two types of binding modes were identified for the ligand (Figure 5).

The binding modes predicted that the carbonyl oxygen (next to the trimethyl group) is able to form hydrogen bonds to the backbone nitrogen of either ALA331 (Figure 5A) or both MET332 and VAL333 (Figure 5B). The triazole ring is also favorably positioned to form hydrogen bonds to the backbone nitrogen of ARG316 (Figure 5A). Furthermore, ALA331, MET332, VAL333, and ARG316 are part of the pocket that surrounds the isoalloxazine moiety of FAD.<sup>70</sup> Occupation of these amino acids may result in the ejection of FAD. To further assess the dynamic stabilities of the predicted binding poses, short (1 ns) MD simulations were also performed on the binding poses of the two ligands. Overall, we found that both binding modes were well maintained during the short MD simulations for the ligands, which is in line with the experimental data showing that compound **26** in the cavity of LSD1 belongs to the FAD-binding subdomain, while Arg 316 is one of the binding sites of FAD.<sup>71</sup> These results further support our findings about the competitive inhibition of compound **26** over FAD, but specific mechanism on how does compound **26** act on LSD1 still needs to be clarified in further structure analysis.

#### Effects of Compounds **22** and **26** on LSD1 Activity in Cultured Gastric Cancer Cells and Their Cytotoxicities.

To determine whether compounds **22** and **26** are cell active LSD1 inhibitors, the effects of these compounds on the methylation levels of LSD1 substrates H3K4 and H3K9 were analyzed in MGC-803 cells. We found that the amounts of H3K4me/me2 and H3K9me2 were dose dependently elevated



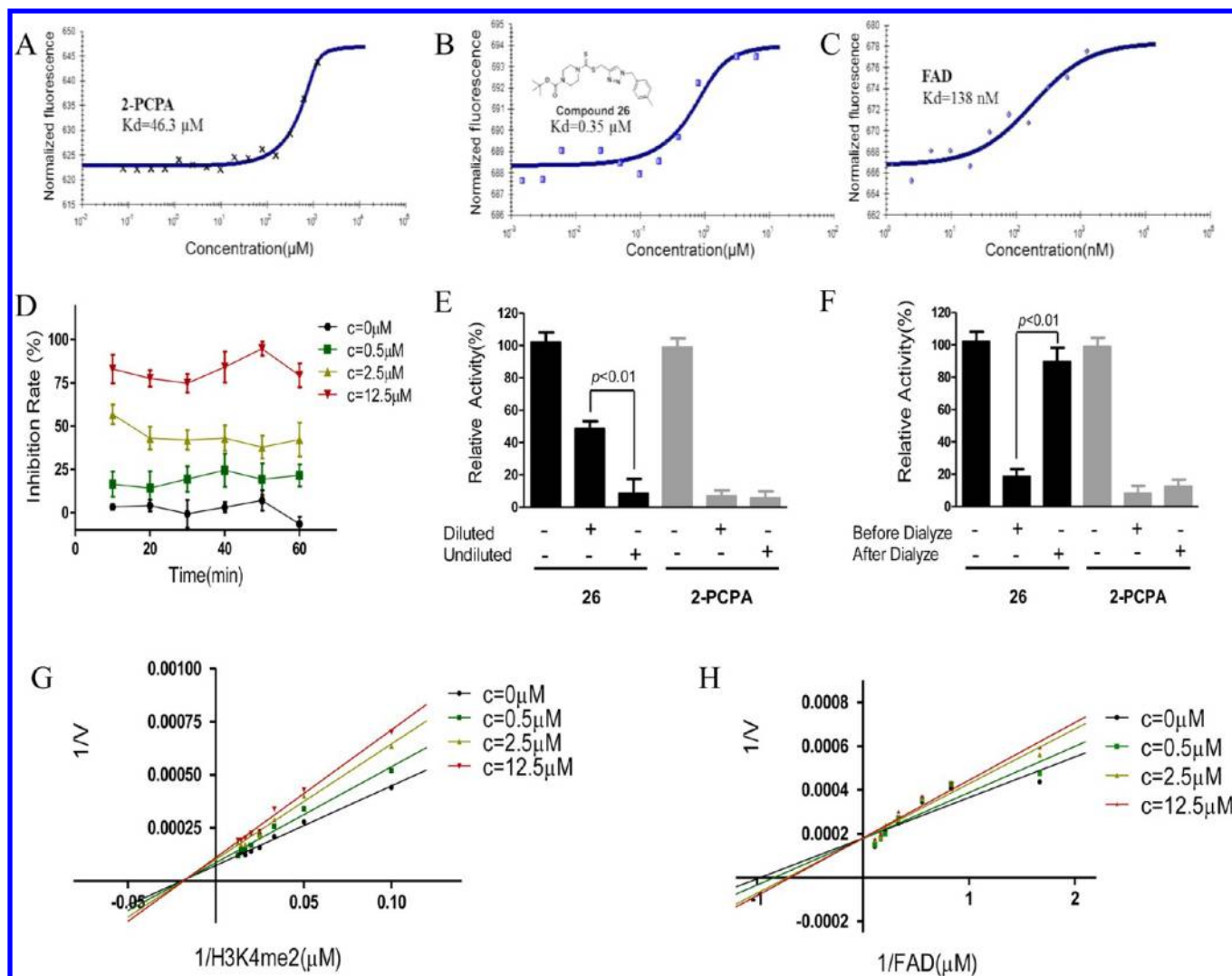


**Figure 4.** Properties of compound 26's inhibitory effect to LSD1 activity in vitro. (A–C)  $K_d$  values for 2-PCPA (A), compounds 26 (B), and FAD (C) were obtained by microscale thermophoresis (MST) experiment. (D) Time dependent assay of compound 26 against LSD1. The stable progress curves for the inactivation of LSD1 were obtained by indicated concentrations of compound 26 treatment. (E, F) The reversibility of compound 26 to LSD1 activity was determined by dilution assay (E) and dialysis experiment (F). 2-PCPA was used a control. (G, H) Lineweaver–Burk plots demonstrate that compound 26 is noncompetitive with the histone H3 substrate (G) and competitive with the LSD1 cofactor FAD (H). Data are the mean  $\pm$  SD.  $P < 0.01$  was considered statistically highly significant. All experiments were carried out at least three times.

**Table 6. In Vitro Inhibitory Activities of Compounds 22, 26 to LSD1 and Its Homologies LSD2, MAO-A, and MAO-B<sup>a</sup>**

compd	$IC_{50} (\mu\text{M})$			
	LSD1	LSD2	MAO-A	MAO-B
22	$11.5 \pm 2.1$	$49.1 \pm 7.3$	$>1250$	$790.7 \pm 10.4$
26	$2.1 \pm 1.1$	$36.6 \pm 4.5$	$>1250$	$>1250$
2-PCPA	$28.7 \pm 3.5$	$34.9 \pm 5.3$	$10.6 \pm 1.0$	$5.9 \pm 0.8$

<sup>a</sup>2-PCPA was used as control.

after treatment of MGC-803 cells with these two compounds (Figure 6). These results validated that compounds 22 and 26 can decrease LSD1 activity at the cellular level. To further determine the specificity of compounds 22 and 26 at the cellular level, the expression level of H3K4me3 that is the substrate of histone demethylase JARID1 was also evaluated. Figure 6A and Figure 6B show that compounds 22 and 26 did not affect the expression of H3K4me3. These results suggested

that compounds 22 and 26 are specific and cell active LSD1 inhibitors.

To further determine whether compounds 22 and 26 are potential candidates for chemotherapeutic agents against gastric cancer, the in vitro cytotoxicities of compounds 22 and 26 were evaluated by MTT method. Both compounds exhibited strong cytotoxicity against human gastric cancer cell lines MGC-803 and HGC-27 with higher LSD1 expression ( $IC_{50}$  of compounds 22 and 26 for MGC-803 line are 1.26 and 0.89  $\mu\text{M}$ , respectively;  $IC_{50}$  of compounds 22 and 26 for HGC-27 cell line are 1.56 and 1.13  $\mu\text{M}$ , respectively) (Figure 7A–D). However, both of them did not show any marked effects on normal gastric epithelial cell line GES-1 and gastric cancer cell line SGC-7901 and both with lower LSD1 expression ( $IC_{50}$  values of compounds 22 and 26 for SGC-7901 cell line are 69.5 and 89.5  $\mu\text{M}$ , respectively;  $IC_{50}$  values of compounds 22 and 26 for GES-1 cell line are 50.26 and 45.26  $\mu\text{M}$ , respectively) (Figure 7A–E). siRNA mediated LSD1 knock down (Figure 7F) in MGC-803 cells also resulted in a loss of cell viability

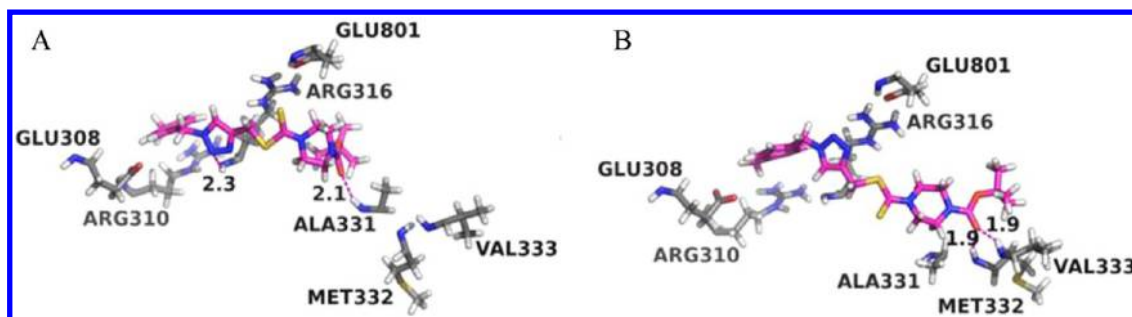


**Figure 5.** Putative binding modes of the ligands **26** in the FAD-binding site of LSD1: (A) **26** pose 1; (B) **26** pose 2. FAD-binding site residues are colored in gray while the ligand **26** is colored in magenta and green, respectively. Hydrogen bonds between the protein and ligands are shown in magenta dash lines with the distances (Å) between the donor hydrogen atom and the acceptor heavy atom labeled.

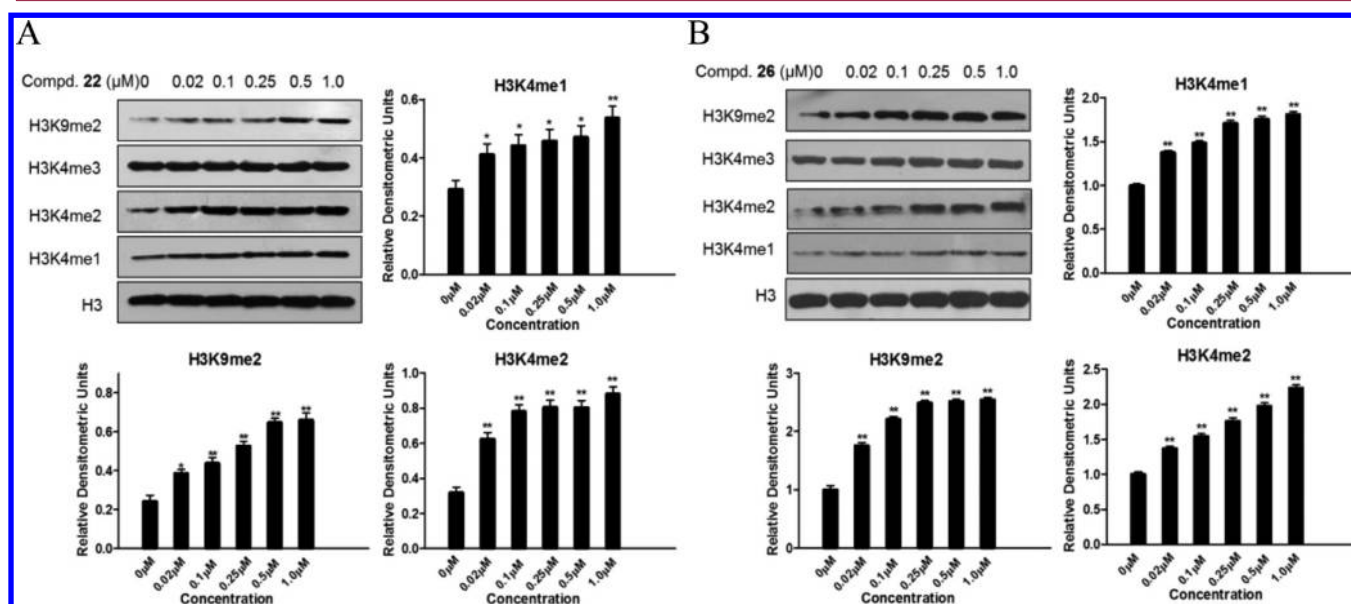


**Figure 6.** Histone methylation in MGC-803 cells after treatment by compound **22** (A) and **26** (B) for 48 h. The expressions of H3K4me1, me2, H3K9me2, and H3K4me3 were then determined by Western blot. The total levels of histone 3 (H3) were used as loading control. Data are the mean  $\pm$  SD. (\*)  $P < 0.05$  was considered significant. (\*\*)  $P < 0.01$  was considered statistically highly significant. All experiments were carried out at least three times.

(Figure 7G). These findings implicated that the cytotoxicities of compounds **22** and **26** on gastric cancer cells may be associated with their specific inhibition to the enhanced LSD1 expression in those cells.

**Effect of Compound 26 on Apoptosis, Cell Migration, and Invasion.** To explore cytotoxicity of **26** in MGC-803 cells, cell apoptosis was investigated with Hoechst 33258 staining. After a 48 h incubation with **26** at indicated concentrations, characteristic apoptotic morphological changes were observed by fluorescence microscope, including cell rounding, chromatin shrinkage, and formation of apoptotic bodies (Figure 8A). The apoptotic analysis was also performed with annexin V-FITC/PI double staining and quantitated by flow cytometry. Compound **26** treatment of MGC-803 cells dose dependently increased the percentage of the apoptotic population up to 12.6%, 31.7%, and 44.7%, respectively, compared to control (7.9%) (Figure 8B,C). As LSD1 shows a strong preference to reverse K370me2 of p53, which inhibits its association with the coactivator 53BP1 (p53-binding protein 1) through tandem Tudor domains in 53BP1 and represses p53 function,<sup>5</sup> we suppose that **26** may prevent the demethylation at K370me2 of p53 by LSD1 and promote p53-mediated apoptosis.

In addition, MGC-803 cell migration was evaluated by wound healing and Transwell experiments. Cell invasion capacity was determined by Matrigel coated Transwell experiment following a reported procedure.<sup>72</sup> Microphotographs showed that untreated gastric cancer MGC-803 cells filled most of the wounded area 2 days after scratching the cell monolayer, whereas treatment with indicated doses of compound **26** markedly suppressed repairment of the wound (Figure 9A). The inhibitory effect of compound **26** on repopulation of the wounded area was not due to decreased proliferation because the highest concentration (0.25  $\mu$ M) of compound **26** we used in this assay cannot inhibit the cell proliferation as we discussed in Figure 8. Compound **26** also significantly inhibited the cell migration and invasion even at low concentration (0.02  $\mu$ M) (Figure 9B,C), so did the siRNA mediated LSD1 knock-down, when compared to the positive control 100  $\mu$ M 2-PCPA (Figure 9B,C). These results indicate that the effect of compound **26** on cell migration and invasion is much more powerful than 2-PCPA. LSD1 can form a complex with snail to act at the E-box domain of E-cadherin and restrain the expression of E-cadherin for promoting cell migration and invasion.<sup>53,54</sup> After incubation with compound **26**, the protein levels of E-cadherin were markedly elevated,

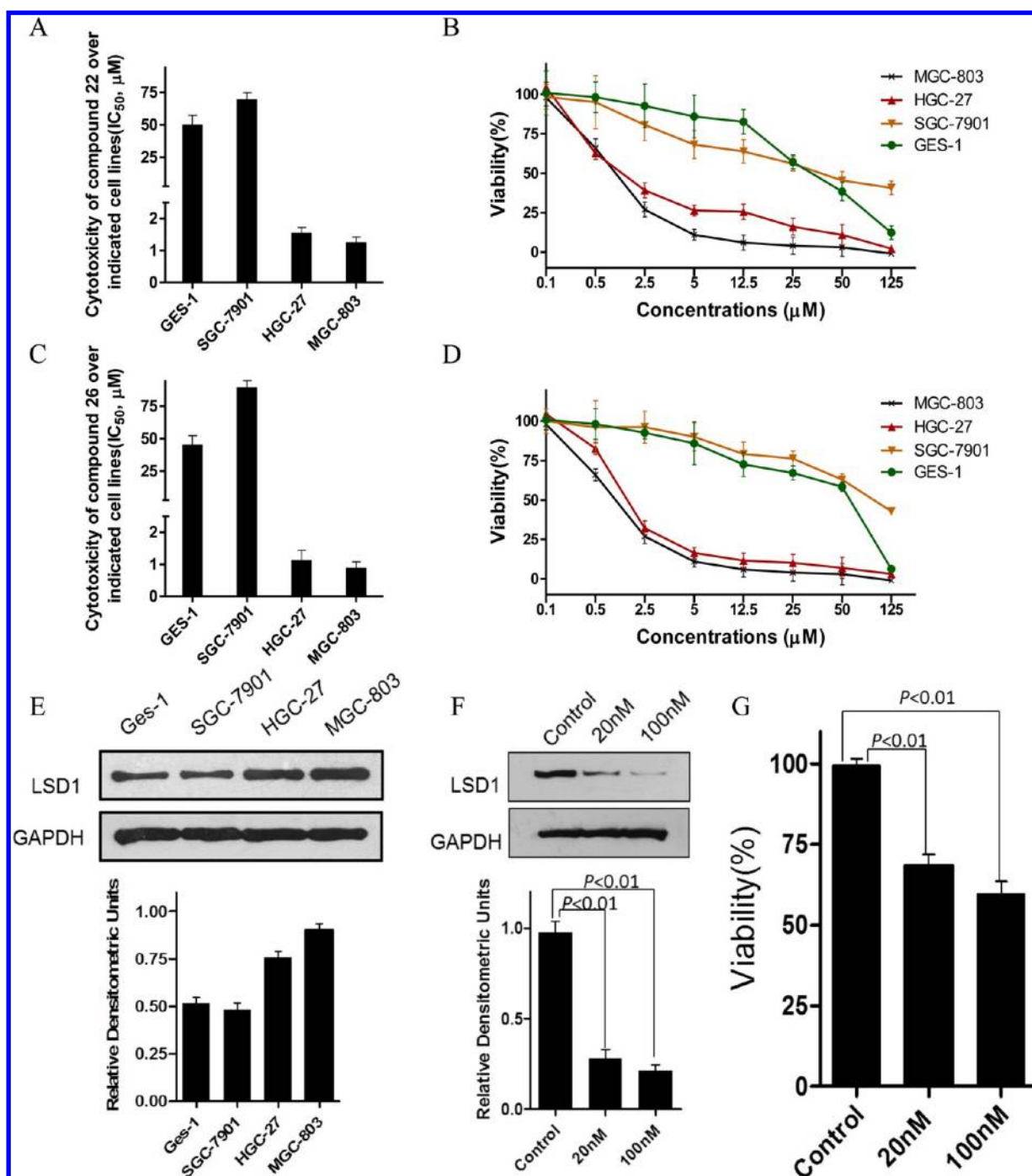


**Figure 7.** IC<sub>50</sub> and cell viability of **22** (A, B), and **26** (C, D) treatment on three gastric cancer cell lines MGC-803, HGC-27, SGC-7901 and normal gastric epithelial cell line GES-1. (E) Expression levels of LSD1 on the four gastric cell lines indicated above. (F) 3 days after LSD1 siRNA transfection in MGC-803 cells; LSD1 protein levels were determined by Western blot, and GAPDH was used as the loading control. (G) Cell viability upon LSD1 siRNA treatment. Data are the mean  $\pm$  SD. (\*\*)  $P < 0.01$  was considered statistically highly significant. All experiments were carried out at least three times.

without significant alteration of the total levels of LSD1 and snail, compared to those on control (Figure 9D,E). To further determine the effects of compound **26** on the complex formation between LSD1 and snail, co-immunoprecipitation was performed, using LSD1 antibody as a bait. After compound **26** treatment for 48 h, the binding of LSD1 to snail was significantly decreased, which is the same as that by the positive control 2-PCPA (Figure 9F,G). These results indicated that the enhanced expression of E-cadherin by compound **26** may be

associated with the decreased interaction of LSD1 and snail and further clarified the inhibitory mechanism on the cell migration and invasion by this compound.

**In Vivo Antitumor Study.** We next examined the effect of compound **26** on tumor growth in vivo in a xenograft model. Xenograft tumors were generated by subcutaneous implantation of MGC-803 cells into nude mice. After the treatment, body weights of the mice were monitored and their tumor sizes were measured and recorded every 3 days (Figure 10A).



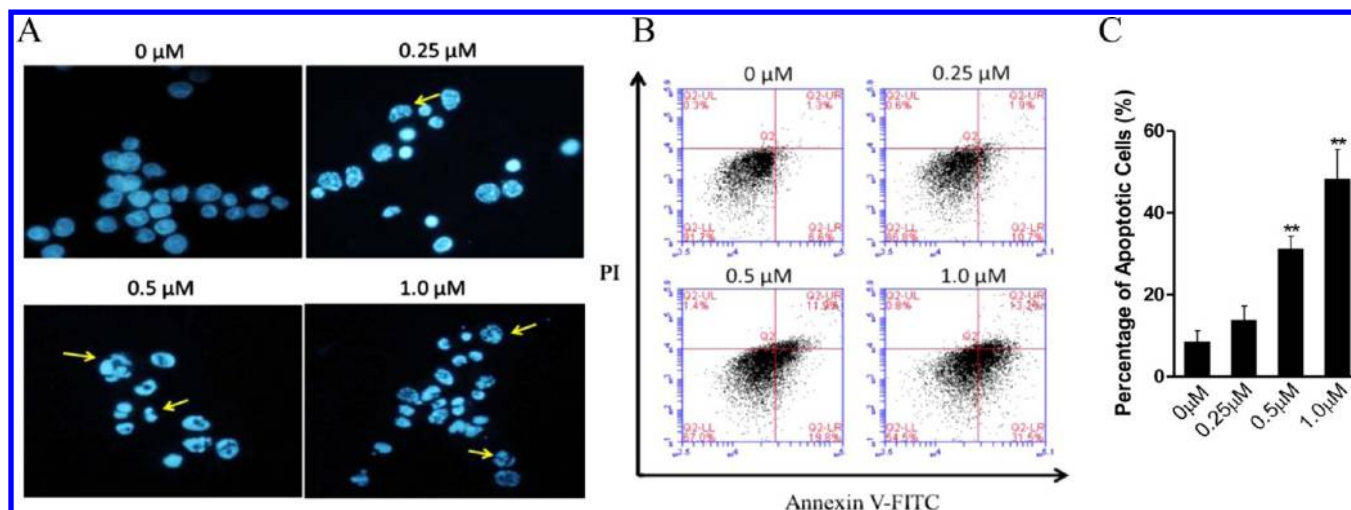


**Figure 8.** Compound **26** induced apoptosis in MGC-803 cells. (A) Apoptosis analysis with Hoechst-33258 staining after a 48 h treatment of **26** in MGC-803 cells. (B, C) Quantitative analysis of apoptotic cells using annexinV-FITC/PI double staining and flow-cytometry calculation. (\*\*)  $P < 0.01$  was considered statistically highly significant. Data are the mean  $\pm$  SD. All experiments were carried out at least three times.

Compound **26** treatment at a dose of 20 mg/kg significantly inhibited the growth of tumor over time and reduced tumor weight by 68.5% (Figure 10A–C). There were no apparent body weight loss during the treatment (Figure 10D). These data indicate that compound **26** was efficacious in inhibiting the growth of LSD1 overexpressing gastric tumor in vivo but no obvious global toxicity.

## CONCLUSION

In summary, we have synthesized and identified a novel class of triazole–dithiocarbamate based selective LSD1 inhibitors. Some of these triazole–dithiocarbamates, especially compound **26**, exhibit reversible and FAD competitive LSD1 inhibition. To our best knowledge, compound **26** is the first identified highly selective LSD1 inhibitor with the ability to inhibit cell migration and invasion at lower concentrations. Our findings indicate that the lead triazole–dithiocarbamate based LSD1 inhibitor may be developed as a novel anticancer epigenetic drug to target gastric cancer with overexpression of LSD1.

## METHODS

**General Methods for Chemistry.** Reagents and solvents were purchased from commercial sources and were used without further purification. Melting points were determined on a X-5 micromelting apparatus, and  $^1\text{H}$  NMR and  $^{13}\text{C}$  NMR spectra were recorded on a Bruker 400 and 100 MHz spectrometer, respectively. IR spectra were recorded on a Nicolet iS10 infrared spectrometer. High resolution mass spectra were recorded on a Waters Micromass Q-T of Micromass spectrometer. The purity of all biologically evaluated compounds was determined to be >95% by reverse phase high performance liquid chromatography (HPLC) analysis. HPLC measurement was performed with a Phenomenex column (C18, 5.0  $\mu\text{m}$ , 4.6 mm  $\times$  150 mm) on Dionex UltiMate 3000 UHPLC instrument from Thermo-Fisher. The signal was monitored at 254 nm with a UV detector. A flow rate of 0.5 mL/min was used with mobile phase of MeOH in  $\text{H}_2\text{O}$  (80:20, v/v).

**General Procedure for the Synthesis of Alkynes 4a–j.**  $\text{CS}_2$  (2.28 g, 30 mmol) was added dropwise to the solution of *tert*-butyl piperazine-1-carboxylate (1.86g, 10 mmol) and  $\text{Na}_3\text{PO}_4 \cdot 12\text{H}_2\text{O}$  (2.28 g, 6 mmol) in acetone (40 mL). The reaction mixture was stirred at room temperature for 0.5 h. Then propargyl bromide (1.31 g, 11 mmol) was added to the mixture dropwise. The reaction mixture was stirred at room temperature for another 0.5 h. Then the reaction

mixture was filtered and the filtrate was concentrated under reduced pressure. The residue was dissolved in EtOAc (50 mL), washed with water (50 mL), brine (50 mL), dried over anhydrous  $\text{Na}_2\text{SO}_4$ , and concentrated under vacuum to afford alkyne **4j**.

**Prop-2-ynyl 4-(2-Hydroxyethyl)piperazine-1-carbodithioate (4c).** Yield 82.2%, white solid. Mp: 96–97  $^\circ\text{C}$ .  $^1\text{H}$  NMR (400 MHz,  $\text{CDCl}_3$ ):  $\delta$  4.36 (brs, 2H), 4.12 (d,  $J = 2.7$  Hz, 2H), 3.96 (brs, 2H), 3.69 (t,  $J = 5.3$  Hz, 2H), 2.64 (m, 6H), 2.27 (t,  $J = 2.7$  Hz, 2H). HRMS (ESI) calcd for  $\text{C}_{10}\text{H}_{17}\text{N}_2\text{OS}_2$   $[\text{M} + \text{H}]^+$ : 245.0782. Found: 245.0781.

***tert*-Butyl 4-((Prop-2-ynylthio)carbonothioyl)piperazine-1-carboxylate (4j).** Yield 92%, white solid. Mp: 87–88  $^\circ\text{C}$ .  $^1\text{H}$  NMR (400 MHz, acetone- $d_6$ , ppm):  $\delta$  4.28 (brs, 2H), 4.14 (d,  $J = 2.7$  Hz, 2H), 4.00 (brs, 2H), 3.58 (brs, 4H), 2.78 (t,  $J = 2.7$  Hz, 1H), 1.46 (s, 9H).  $^{13}\text{C}$  NMR (100 MHz,  $\text{CDCl}_3$ , ppm):  $\delta$  195.16, 154.39, 80.68, 78.19, 71.82, 28.36, 26.00. HRMS (ESI) calcd for  $\text{C}_{13}\text{H}_{21}\text{N}_2\text{O}_2\text{S}_2$   $[\text{M} + \text{H}]^+$ : 301.1044. Found: 301.1046.

### General Procedure for the Synthesis of Compounds 12–72.

In a round-bottom flask equipped with a magnetic stirred bar, alkyne derivatives **4** (5 mmol), azide derivatives **5** (5.5 mmol),  $\text{CuSO}_4 \cdot 5\text{H}_2\text{O}$  (62 mg, 0.25 mmol), sodium ascorbate (100 mg, 0.5 mmol), THF (20 mL), and  $\text{H}_2\text{O}$  (20 mL) were added. The resulting mixture was stirred at room temperature for about 2 h. The disappearance of compounds **4** was monitored by TLC (silica gel, PE/EtOAc = 3:1). After the reaction, water (40 mL) was added and the reaction mixture was extracted with EtOAc (3  $\times$  40 mL). The combined organic layer was washed with brine (100 mL), dried over anhydrous  $\text{Na}_2\text{SO}_4$ , and concentrated under vacuum to afford the crude products. The crude products were recrystallized from acetone to yield the pure products **12–72**.

***tert*-Butyl 4-(((1-(2-Fluorobenzyl)-1H-1,2,3-triazol-4-yl)-methylthio)carbonothioyl)piperazine-1-carboxylate (22).** Yield 79.0%, white solid. Mp: 109–110  $^\circ\text{C}$ . IR (KBr,  $\text{cm}^{-1}$ ): 3447, 2979, 1693, 1494, 1478, 1424, 1279, 1167, 1012, 986, 932, 791, 757, 695.  $^1\text{H}$  NMR (400 MHz,  $\text{CDCl}_3$ ):  $\delta$  7.66 (s, 1H), 7.09–7.38 (m, 4H), 5.55 (s, 2H), 4.69 (s, 2H), 4.29 (brs, 2H), 3.91 (brs, 2H), 3.54 (t,  $J = 5.1$  Hz, 4H), 1.47 (s, 9H).  $^{13}\text{C}$  NMR (100 MHz,  $\text{CDCl}_3$ ):  $\delta$  196.42, 161.72, 159.26, 154.41, 144.00, 130.89, 130.81, 130.51, 130.48, 124.82, 124.78, 122.96, 121.98, 121.84, 115.92, 115.71, 80.63, 47.66, 47.61, 31.84, 28.34.  $^{19}\text{F}$  NMR (376 MHz,  $\text{CDCl}_3$ )  $\delta$  –118.03. HRMS (ESI) calcd for  $\text{C}_{20}\text{H}_{27}\text{FN}_5\text{O}_2\text{S}_2$   $[\text{M} + \text{H}]^+$ : 452.1590. Found: 452.1598.

***tert*-Butyl 4-(((1-(4-Fluorobenzyl)-1H-1,2,3-triazol-4-yl)-methylthio)carbonothioyl)piperazine-1-carboxylate (23).** Yield 81.5%, white solid. Mp: 171–172  $^\circ\text{C}$ . IR (KBr,  $\text{cm}^{-1}$ ): 3482, 3139, 2974, 1690, 1470, 1420, 1281, 1167, 1051, 994, 824, 781, 541.  $^1\text{H}$  NMR (400 MHz,  $\text{CDCl}_3$ , ppm):  $\delta$  7.59 (s, 1H), 7.04–7.27 (m, 4H), 5.46 (s, 2H), 4.68 (s, 2H), 4.31 (brs, 2H), 3.90 (brs, 2H), 3.53 (s, 4H),

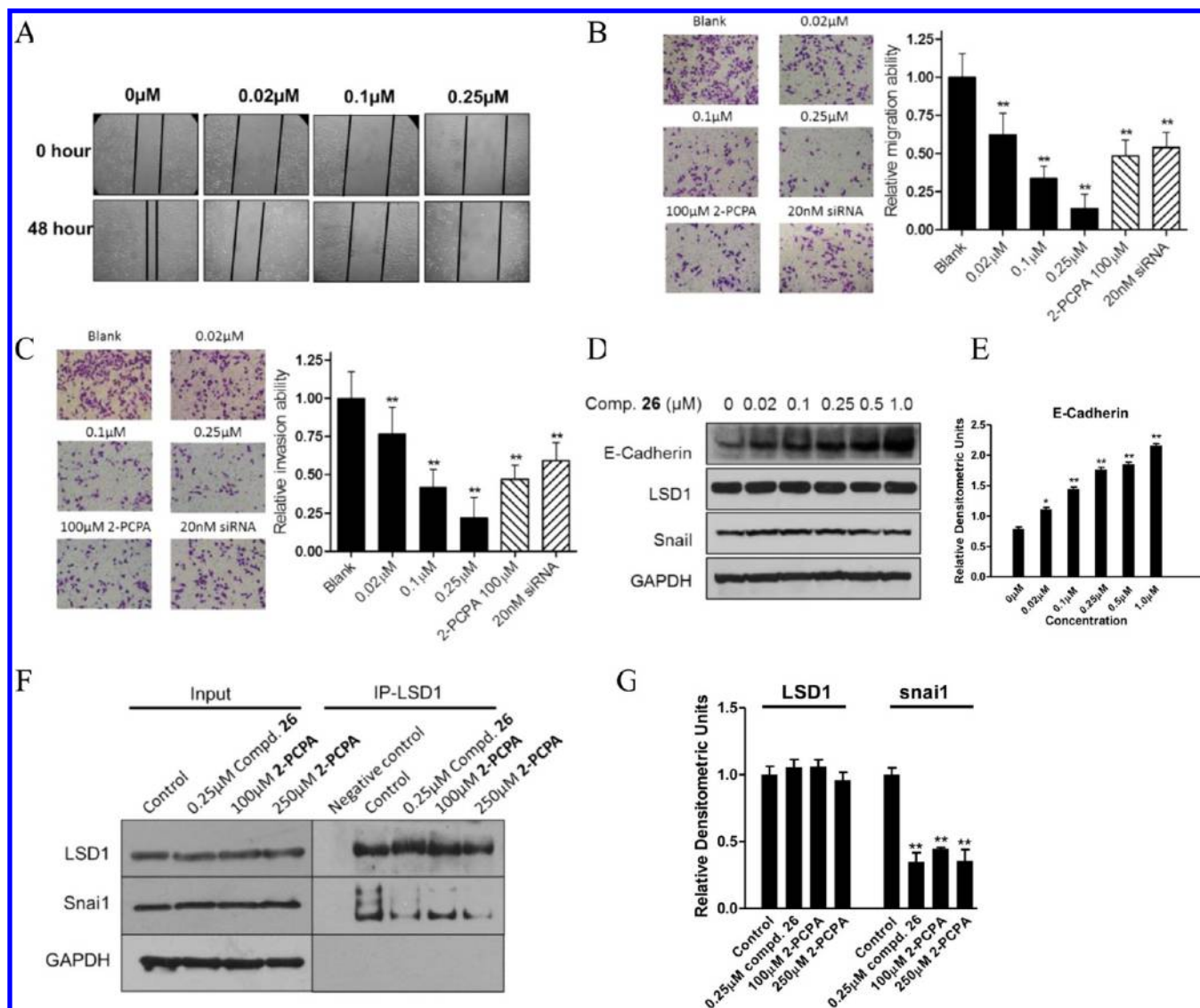


**Figure 9.** Effects of compound **26** on cell migration, invasion in MGC-803 cells. (A) Wound healing assay. (B, C) Migration and invasion ability assay. Treatment of both compound **26** and LSD1 siRNA resulted in the depressed migration (B) and invasion (C) ability in MGC-803 cells. 2-PCPA was used as the positive control. (D and E) The expressions of E-cadherin, snail, and LSD1 after a 48 h treatment of compound **26**. (F, G) Immunoprecipitation and densitometry quantitation of LSD1 and snail without (control) or with compound **26** and 100 and 250 μM 2-PCPA treatment in MGC-803 cells; input represents cell lysate controls. GAPDH was used as loading control. (\*)  $P < 0.05$  was considered statistically significant. (\*\*)  $P < 0.01$  was considered statistically highly significant. Data are the mean  $\pm$  SD. All experiments were carried out at least three times.

1.47 (s, 9H).  $^{13}\text{C}$  NMR (100 MHz,  $\text{CDCl}_3$ , ppm):  $\delta$  196.40, 164.07, 161.60, 154.40, 130.49, 130.45, 129.96, 129.87, 116.20, 115.98, 80.66, 53.42, 31.78, 28.34.  $^{19}\text{F}$  NMR (376 MHz,  $\text{CDCl}_3$ )  $\delta$  -112.68. HRMS (ESI) calcd for  $\text{C}_{20}\text{H}_{27}\text{FN}_5\text{O}_2\text{S}_2$   $[\text{M} + \text{H}]^+$ : 452.1590. Found: 452.1588.

**tert-Butyl 4-(((1-(2-Chlorobenzyl)-1*H*,1,2,3-triazol-4-yl)-methylthio)carbonothioyl)piperazine-1-carboxylate (24).** Yield 78.7%, white solid. Mp: 105–106 °C.  $^1\text{H}$  NMR (400 MHz,  $\text{CDCl}_3$ , ppm):  $\delta$  7.70 (s, 1H), 7.46 (dd,  $J_1 = 1.4$  Hz,  $J_2 = 7.8$  Hz, 1H), 7.23–7.33 (m, 2H), 7.18 (dd,  $J_1 = 1.6$  Hz,  $J_2 = 7.4$  Hz, 1H), 5.62 (s, 2H), 4.70 (s, 2H), 4.28 (brs, 2H), 3.93 (brs, 2H), 3.54 (t,  $J = 5.2$  Hz, 4H), 1.47 (s, 9H).  $^{13}\text{C}$  NMR (100 MHz, acetone- $d_6$ , ppm):  $\delta$  195.68, 154.33, 143.01, 133.30, 133.16, 130.60, 130.31, 129.74, 127.71, 123.79, 79.78, 50.99, 31.63, 27.63. HRMS (ESI) calcd for  $\text{C}_{20}\text{H}_{27}\text{ClN}_5\text{O}_2\text{S}_2$   $[\text{M} + \text{H}]^+$ : 468.1295. Found: 468.1292.

**tert-Butyl 4-(((1-(4-Methylbenzyl)-1*H*,1,2,3-triazol-4-yl)-methylthio)carbonothioyl)piperazine-1-carboxylate (26).** Yield 81.9%, white solid. Mp: 182–183 °C. IR (KBr,  $\text{cm}^{-1}$ ): 3454, 2975, 1682, 1457, 1422, 1224, 1078, 994, 933, 867, 772, 524;  $^1\text{H}$  NMR (400

MHz,  $\text{CDCl}_3$ , ppm):  $\delta$  7.55 (s, 1H), 7.16–7.21 (m, 4H), 5.43 (s, 2H), 4.67 (s, 2H), 4.29 (brs, 2H), 3.91 (brs, 2H), 3.54 (t,  $J = 5.2$  Hz, 4H), 2.35 (s, 3H), 1.47 (s, 9H).  $^{13}\text{C}$  NMR (100 MHz,  $\text{CDCl}_3$ , ppm):  $\delta$  196.49, 154.41, 138.67, 131.57, 129.75, 128.09, 80.64, 54.01, 31.91, 28.35, 21.15. HRMS (ESI) calcd for  $\text{C}_{21}\text{H}_{30}\text{N}_5\text{O}_2\text{S}_2$   $[\text{M} + \text{H}]^+$ : 448.1841. Found: 448.1840.

**tert-Butyl 4-(((1-(4-Methoxybenzyl)-1*H*,1,2,3-triazol-4-yl)-methylthio)carbonothioyl)piperazine-1-carboxylate (27).** Yield 85.8%, white solid. Mp: 129–130 °C.  $^1\text{H}$  NMR (400 MHz,  $\text{CDCl}_3$ , ppm):  $\delta$  7.54 (s, 1H), 7.21 (d,  $J = 8.7$  Hz, 2H), 6.88 (d,  $J = 8.7$  Hz, 2H), 5.41 (s, 2H), 4.67 (s, 2H), 4.29 (brs, 2H), 3.90 (brs, 2H), 3.80 (s, 3H), 3.51 (t,  $J = 5.2$  Hz, 4H), 1.47 (s, 9H).  $^{13}\text{C}$  NMR (100 MHz,  $\text{CDCl}_3$ , ppm):  $\delta$  196.47, 159.89, 154.40, 143.86, 129.62, 126.59, 122.52, 114.44, 80.61, 55.34, 53.70, 31.90, 28.35. HRMS (ESI) calcd for  $\text{C}_{21}\text{H}_{30}\text{N}_5\text{O}_3\text{S}_2$   $[\text{M} + \text{H}]^+$ : 464.1790. Found: 464.1794.

**tert-Butyl 4-(((1-(2-Bromobenzyl)-1*H*,1,2,3-triazol-4-yl)-methylthio)carbonothioyl)piperazine-1-carboxylate (32).** Yield 79.0%, white solid. Mp: 129–130 °C.  $^1\text{H}$  NMR (400 MHz,  $\text{CDCl}_3$ , ppm):  $\delta$  7.71 (s, 1H), 7.62 (dd,  $J_1 = 1.1$  Hz,  $J_2 = 7.9$  Hz, 1H), 7.32 (td,



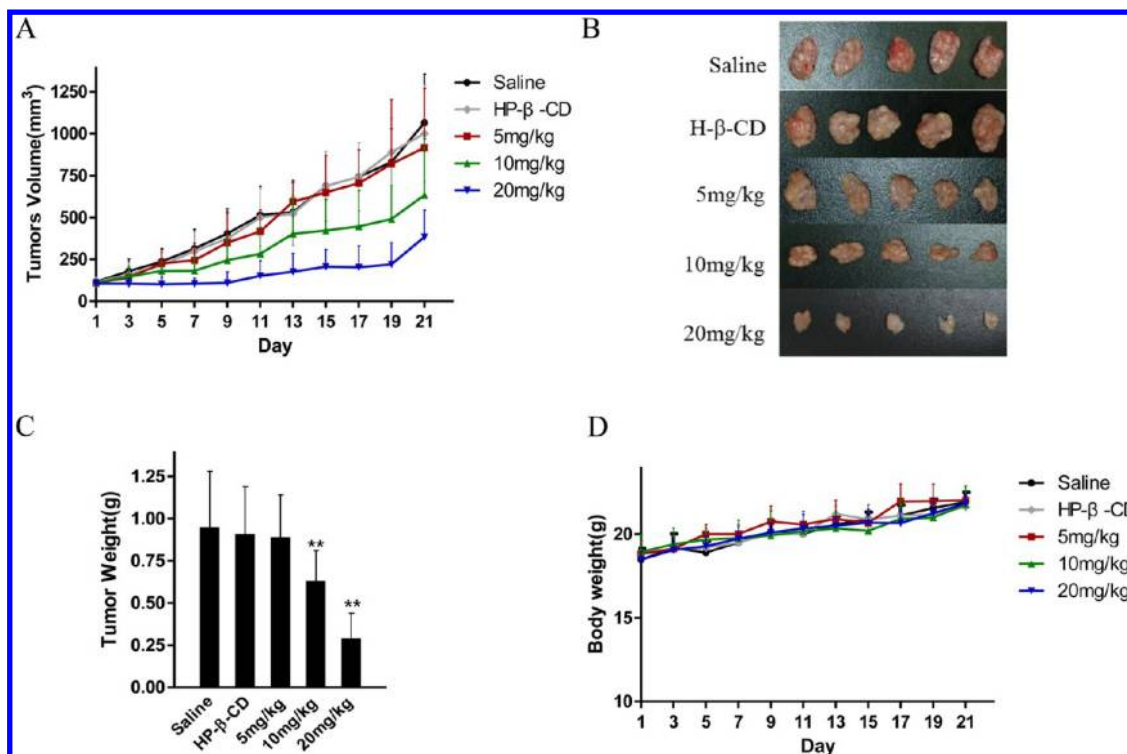


**Figure 10.** In vivo antitumor effects of compound **26** in MGC-803 bearing nude mice. MGC-803 cells were transplanted subcutaneously to the BALB-C nude mice and subjected to saline, hydroxypropyl- $\beta$ -cyclodextrin (HP- $\beta$ -CD), and compound **26** (5, 10, 20 mg/kg) for 21 days, respectively, and were then analyzed for tumor volume (A). (B) Represented tumors with the indicated treatment. (C) Tumor weight with the indicated treatment. (D) Body weight with the indicated treatment. (\*\*)  $P < 0.01$  was considered statistically highly significant. Data are the mean  $\pm$  SD.

$J_1 = 1.1$  Hz,  $J_2 = 7.5$  Hz, 1H), 7.24 (td,  $J_1 = 1.5$  Hz,  $J_2 = 7.8$  Hz, 1H), 7.12 (dd,  $J_1 = 1.5$  Hz,  $J_2 = 7.6$  Hz, 1H), 5.62 (s, 2H), 4.69 (s, 2H), 4.30 (brs, 2H), 3.92 (brs, 2H), 3.54 (t,  $J = 4.8$  Hz, 4H), 1.47 (s, 9H).  $^{13}\text{C}$  NMR (100 MHz,  $\text{CDCl}_3$ ,  $\delta$ , ppm): 196.4, 154.4, 134.2, 133.2, 130.3, 130.2, 128.2, 123.4, 80.6, 53.8, 31.9, 28.4. HRMS (ESI) calcd for  $\text{C}_{20}\text{H}_{27}\text{BrN}_5\text{O}_2\text{S}_2$  [ $\text{M} + \text{H}$ ] $^+$ : 512.0790. Found: 512.0793.

**General Procedure for the Synthesis of Compounds 73–82.**  $\text{CF}_3\text{COOH}$  (4.56 g, 40 mmol) was added to a solution of **22** (0.90 g, 2 mmol) in  $\text{CH}_2\text{Cl}_2$  (20 mL) at 0 °C. The reaction mixture was warmed to room temperature and stirred at the same temperature for about 8 h. The disappearance of compounds **22** was monitored by TLC (silica gel,  $\text{CH}_2\text{Cl}_2/\text{CH}_3\text{OH} = 8:1$ ). The reaction mixture was concentrated under vacuum. The residue was dissolved in  $\text{CH}_2\text{Cl}_2$  (20 mL), washed with saturated  $\text{NaHCO}_3$  (50 mL), brine (50 mL), dried over anhydrous  $\text{Na}_2\text{SO}_4$ , and concentrated under vacuum to afford compounds **73**, which were used in the next reaction without further purification.

**(1-(2-Fluorobenzyl)-1H-1,2,3-triazol-4-yl)methyl Piperazine-1-carbodithioate (73).** Yield 96.7%, white solid. Mp: 93–94 °C.  $^1\text{H}$  NMR (400 MHz,  $\text{CDCl}_3$ , ppm):  $\delta$  7.67 (s, 1H), 7.34–7.40 (m, 1H), 7.24–7.26 (m, 1H), 7.11–7.18 (m, 2H), 5.55 (s, 2H), 4.69 (s, 2H), 4.30 (brs, 2H), 3.93 (brs, 2H), 2.96 (t,  $J = 4.8$  Hz, 4H).  $^{13}\text{C}$  NMR (100 MHz,  $\text{CDCl}_3$ , ppm):  $\delta$  195.81, 161.72, 159.26, 144.27, 130.88, 130.80, 130.50, 130.47, 124.82, 124.79, 122.98, 122.00, 121.86, 115.93, 115.72, 47.66, 47.61, 45.58, 31.76. HRMS (ESI) calcd for  $\text{C}_{15}\text{H}_{19}\text{FN}_5\text{S}_2$  [ $\text{M} + \text{H}$ ] $^+$ : 352.1066. Found: 352.1064.

**1-(4-Methylbenzyl)-1H-1,2,3-triazol-4-yl)methyl Piperazine-1-carbodithioate (78).** Yield 94.0%, white solid. Mp: 74–75 °C.  $^1\text{H}$  NMR (400 MHz,  $\text{CDCl}_3$ , ppm):  $\delta$  7.56 (s, 1H), 7.18 (s, 4H), 5.43 (s, 2H), 4.67 (s, 2H), 4.31 (brs, 2H), 3.92 (brs, 2H), 2.96 (brs, 4H), 2.35 (s, 3H).  $^{13}\text{C}$  NMR (100 MHz,  $\text{CDCl}_3$ , ppm):  $\delta$  195.82, 138.61, 131.59, 129.74, 128.08, 122.72, 53.96, 31.80, 29.68, 21.17. HRMS (ESI) calcd for  $\text{C}_{16}\text{H}_{22}\text{N}_5\text{S}_2$  [ $\text{M} + \text{H}$ ] $^+$ : 348.1317. Found: 348.1319.

**(1-(4-Methoxybenzyl)-1H-1,2,3-triazol-4-yl)methyl Piperazine-1-carbodithioate (79).** Yield 92.7%, white solid. Mp: 95–96

°C.  $^1\text{H}$  NMR (400 MHz,  $\text{CDCl}_3$ , ppm):  $\delta$  7.55 (s, 1H), 7.24 (d,  $J = 8.7$  Hz, 2H), 6.91 (d,  $J = 8.7$  Hz, 2H), 5.42 (s, 2H), 4.68 (s, 2H), 4.31 (brs, 2H), 3.95 (brs, 2H), 3.80 (s, 3H), 2.96 (t,  $J = 4.6$  Hz, 4H).  $^{13}\text{C}$  NMR (100 MHz,  $\text{CDCl}_3$ , ppm):  $\delta$  195.8, 159.9, 144.1, 129.6, 126.6, 122.5, 114.5, 55.3, 53.7, 45.6, 31.8. HRMS (ESI) calcd for  $\text{C}_{16}\text{H}_{22}\text{N}_5\text{O}_2\text{S}_2$  [ $\text{M} + \text{H}$ ] $^+$ : 364.1266. Found: 364.1263.

**General Procedure for the Synthesis of Compounds 83–92.** A mixture of **73** (0.70 g, 2 mmol),  $\text{K}_2\text{CO}_3$  (0.28 g, 2 mmol), and  $\text{CbzCl}$  (0.38 g, 2.2 mol) in  $\text{CH}_2\text{Cl}_2$  (20 mL) was stirred at room temperature for 7 h. The disappearance of compounds **73** was monitored by TLC (silica gel,  $\text{PE}/\text{acetone} = 3:1$ ). After the reaction,  $\text{K}_2\text{CO}_3$  was removed by filtration and the solvent was diluted with  $\text{CH}_2\text{Cl}_2$  (10 mL), washed with water (40 mL), brine (40 mL), dried over anhydrous  $\text{Na}_2\text{SO}_4$ , and concentrated under vacuum to give the crude product, which was recrystallized from acetone to provide compound **83** as a white solid.

**Benzyl 4-(((1-(2-Fluorobenzyl)-1H-1,2,3-triazol-4-yl)-methylthio)carbonothioyl)piperazine-1-carboxylate (83).** Yield 74.6%, white solid. Mp: 138–139 °C.  $^1\text{H}$  NMR (400 MHz,  $\text{CDCl}_3$ , ppm):  $\delta$  7.66 (s, 1H), 7.08–7.37 (m, 9H), 5.54 (s, 2H), 5.15 (s, 2H), 4.69 (s, 2H), 4.30 (brs, 2H), 3.95 (brs, 2H), 3.61 (t,  $J = 5.2$  Hz, 4H).  $^{13}\text{C}$  NMR (100 MHz,  $\text{CDCl}_3$ , ppm):  $\delta$  196.61, 161.73, 159.27, 155.04, 143.97, 136.21, 130.94, 130.85, 130.54, 130.51, 128.61, 128.30, 128.09, 124.84, 124.80, 123.04, 121.93, 121.79, 115.94, 115.73, 67.64, 47.72, 47.68, 43.02, 31.85. HRMS (ESI) calcd for  $\text{C}_{23}\text{H}_{25}\text{FN}_5\text{O}_2\text{S}_2$  [ $\text{M} + \text{H}$ ] $^+$ : 486.1434. Found: 486.1432.

**Benzyl 4-(((1-(4-Methylbenzyl)-1H-1,2,3-triazol-4-yl)-methylthio)carbonothioyl)piperazine-1-carboxylate (87).** Yield 81.8%, white solid. Mp: 99–100 °C.  $^1\text{H}$  NMR (400 MHz,  $\text{CDCl}_3$ , ppm):  $\delta$  7.55 (s, 1H), 7.14–7.37 (m, 9H), 5.44 (s, 2H), 5.16 (s, 2H), 4.67 (s, 2H), 4.29 (brs, 2H), 3.96 (brs, 2H), 3.59 (t,  $J = 5.1$  Hz, 4H), 2.35 (s, 3H).  $^{13}\text{C}$  NMR (100 MHz,  $\text{CDCl}_3$ , ppm):  $\delta$  196.67, 155.04, 138.68, 136.21, 131.56, 129.76, 128.61, 128.31, 128.10, 122.73, 67.64, 54.02, 43.03, 31.95, 21.17. HRMS (ESI) calcd for  $\text{C}_{24}\text{H}_{28}\text{N}_5\text{O}_2\text{S}_2$  [ $\text{M} + \text{H}$ ] $^+$ : 482.1684. Found: 482.1683.

**Benzyl 4-(((1-(3,4,5-Trimethoxybenzyl)-1H-1,2,3-triazol-4-yl)methylthio)carbonothioyl)piperazine-1-carboxylate (90).** Yield 82.0%, white solid. Mp: 134–135 °C. <sup>1</sup>H NMR (400 MHz, CDCl<sub>3</sub>, ppm): δ 7.63 (s, 1H), 7.35–7.37 (m, 5H), 6.47 (s, 2H), 5.40 (s, 2H), 5.15 (s, 2H), 4.68 (s, 2H), 4.28 (brs, 2H), 3.96 (brs, 2H), 3.83 (s, 3H), 3.82 (s, 6H), 3.62 (t, *J* = 5.0 Hz, 4H). <sup>13</sup>C NMR (100 MHz, CDCl<sub>3</sub>, ppm): δ 196.60, 155.02, 153.69, 144.02, 138.30, 136.19, 130.08, 128.60, 128.30, 128.09, 122.82, 105.23, 67.64, 60.85, 56.25, 54.38, 43.01, 31.86. HRMS (ESI) calcd for C<sub>26</sub>H<sub>32</sub>N<sub>5</sub>O<sub>5</sub>S<sub>2</sub> [M + H]<sup>+</sup>: 558.1845. Found: 558.1841.

**Ethyl 4-(((1-(4-Methylbenzyl)-1H-1,2,3-triazol-4-yl)methylthio)carbonothioyl)piperazine-1-carboxylate (91).** Compound **91** was prepared from **77** and ethyl chloroformate using the method above. Yield 77.4%, white solid. Mp: 100–101 °C. <sup>1</sup>H NMR (400 MHz, CDCl<sub>3</sub>, ppm): δ 7.57 (s, 1H), 7.17 (s, 4H), 5.44 (s, 2H), 4.70 (s, 2H), 4.31 (brs, 2H), 4.20 (q, *J* = 7.1 Hz, 2H), 3.93 (brs, 2H), 3.58 (s, 4H), 2.35 (s, 3H), 1.29 (t, *J* = 7.1 Hz, 3H). <sup>13</sup>C NMR (100 MHz, CDCl<sub>3</sub>, ppm): δ 196.60, 155.25, 143.98, 138.70, 131.47, 129.77, 128.13, 122.82, 61.91, 54.08, 42.90, 31.85, 21.18, 14.65. HRMS (ESI) calcd for C<sub>19</sub>H<sub>26</sub>N<sub>5</sub>O<sub>5</sub>S<sub>2</sub> [M + H]<sup>+</sup>: 420.1528. Found: 420.1527.

**Isopropyl 4-(((1-(4-Methylbenzyl)-1H-1,2,3-triazol-4-yl)methylthio)carbonothioyl)piperazine-1-carboxylate (92).** Compound **92** was prepared from **77** and isopropyl chloroformate using the method above. Yield 84.5%. Mp: 149–150 °C. <sup>1</sup>H NMR (400 MHz, CDCl<sub>3</sub>, ppm): δ 7.55 (s, 1H), 7.17 (s, 4H), 5.44 (s, 2H), 4.97 (m, 1H), 4.67 (s, 2H), 4.31 (brs, 2H), 3.93 (brs, 2H), 3.56 (s, 4H), 2.35 (s, 3H), 1.26 (d, *J* = 6.2 Hz, 6H). <sup>13</sup>C NMR (100 MHz, CDCl<sub>3</sub>, ppm): δ 196.56, 154.91, 143.88, 138.66, 131.57, 129.75, 128.10, 122.65, 69.41, 53.97, 42.84, 31.90, 22.21, 21.18. HRMS (ESI) calcd for C<sub>20</sub>H<sub>27</sub>N<sub>5</sub>NaO<sub>5</sub>S<sub>2</sub> [M + Na]<sup>+</sup>: 456.1504. Found: 456.1503.

#### General Procedure for the Synthesis of Compounds 93–95.

A mixture of **73** (0.70g, 2 mmol), Et<sub>3</sub>N (0.76g, 2.2 mmol), and CH<sub>3</sub>COCl (0.17g, 2.2 mol) in CH<sub>2</sub>Cl<sub>2</sub> (10 mL) was stirred at room temperature for 4.5 h. The disappearance of compounds **73** was monitored by TLC (silica gel, PE/acetone = 3:1). After the reaction, the solvent was washed with diluted hydrochloric acid, saturated NaHCO<sub>3</sub> (40 mL), and brine (40 mL), dried over anhydrous Na<sub>2</sub>SO<sub>4</sub>, and concentrated under vacuum to give the crude product, which was recrystallized from acetone to provide compound **93** as white solid.

**(1-(2-Fluorobenzyl)-1H-1,2,3-triazol-4-yl)methyl 4-Acetylpi-piperazine-1-carbodithioate (93).** Yield 71.3%, white solid. <sup>1</sup>H NMR (400 MHz, CDCl<sub>3</sub>): δ 7.67 (s, 1H), 7.09–7.38 (m, 4H), 5.55 (s, 2H), 4.68 (s, 2H), 4.30 (brs, 2H), 4.00 (brs, 2H), 3.73 (t, *J* = 5.1 Hz, 2H), 3.60 (t, *J* = 5.1 Hz, 2H), 2.13 (s, 3H). HRMS (ESI) calcd for C<sub>17</sub>H<sub>20</sub>FN<sub>3</sub>NaOS<sub>2</sub> [M + Na]<sup>+</sup>: 416.0991. Found: 416.0988.

**Cells and Cell Viability Assay.** The human gastric carcinoma cell lines MGC-803 and HGC-27 were supplied by the Cell Bank of Shanghai Institute of Cell Biology, Chinese Academy of Sciences. Human gastric carcinoma cell line SGC-7901 was purchased from Shanghai Bogoo Biotechnology Company. Human gastric epithelial mucosa cell line GES-1 was preserved in our institute. Cells were cultured in DMEM medium or RPMI-1640 medium. All media were supplemented with 10% FBS. Cells were cultured in an incubator with 5% CO<sub>2</sub> at 37 °C with medium changes every 2 days.

The cell viability was determined by 3-(4,5-dimethylthiazol-2-yl)-2,5-diphenyltetrazolium bromide (MTT) assay according to the manufacturer's instructions. This assay measures dehydrogenase enzyme activity in metabolically active tumor cells, as reflected by the conversion of MTT to formazan, which is soluble in tissue culture medium and is detected by absorbance (*A*) at 570 nm. The production of formazan is proportional to the number of living cells, with the intensity of the produced color serving as an indicator of cell viability. The data were analyzed with SPSS 20.

**Inhibitory Evaluation of the Synthesized Compounds against LSD1, LSD2, MAO-A, MAO-B and Mechanism of Action Studies.** cDNA encoding LSD1(157–852AA) was obtained by RT-PCR and cloned into pET28b to have the constructed plasmid pET28b-LSD1. Then the plasmid was transfected into BL21(DE). The recombinant was induced with 0.25 mM IPTG at 20 °C and purified as published, as well as pET28a-LSD2, which is a kindly gift from Dr.

Chen.<sup>18,69</sup> Then the compounds were incubated with the recombinant and H3K4me2. After that, the fluorescence was measured at excitation wavelength 530 nm and emission wavelength 590 nm as reported in order to evaluate the inhibition rate of the candidate compound.<sup>73</sup> Inhibitory effects of the candidate compounds against MAO-A and MAO-B were evaluated with the commercialized kit.

The dilution assay was done as published.<sup>21</sup> Briefly, an amount of 2.5 μg of LSD1 recombinant was incubated with 312.5 μM compound **26**, 600 μM tranlycypromine, or DMSO. At 1 h later, 1.25 μL aliquots were removed from all samples and diluted into HRP-assay solution containing substrate and coupling reagents to a final volume of 100 μL. This represents an 80-fold dilution of the inhibitor concentration, which is expected to yield the same inhibition rate for an irreversible inhibitor or significant difference for a reversible inhibitor.

For the dialysis experiment, compound **26** and LSD1 were incubated for 1 h at 37 °C and then dialyzed against the hepes buffer at 4 °C for 24 h. The buffer was changed every 12 h. Another two groups without inhibitor or with 2-PCPA served as negative or positive controls. Then the activity of LSD1 in the dialyzed tube was measured to evaluate the reversibility of compound **26** inhibitory. Another dialysis experiment was performed, using FAD and LSD1 incubated with or without the inhibitor against hepes buffer at 4 °C for 24 h. In the inhibitor treatment group, the concentrations of inhibitors on both sides of dialysis tube were the same. Then the amount of FAD in the dialysis tubes was measured at 468 nm with a UV/vis spectrophotometer.

For the competitive analysis of compound **26**, demethylase activity of LSD1 was assessed in the presence of different concentrations of the compound (0, 0.5, 2.5, and 12.5 μM) at a fixed concentration of FAD (2.5 μM) and peptide concentrations from 10 to 80 μM or fixed concentration of peptide (25 μM) and FAD concentrations from 0.6 to 9.0 μM. Assays were performed triplicate, and kinetics values were obtained using Lineweaver–Burk plots.<sup>59</sup>

**MST Experiment.** The LSD1 recombinant from Millipore was labeled with a red fluorescent dye using a commercialized kit. The thermophoretic movement of the fluorescently labeled protein in complex with selected inhibitors was measured by monitoring the fluorescence distribution inside the capillary. The concentration of the labeled protein was kept constant at ~200 nM, while the concentration of the compound was varied. The samples were loaded into MST-grade glass capillaries. After a short incubation period, the MST analysis was performed using the Monolith NT.115.

**Docking and Molecular Dynamics Simulations.** The initial coordinates of LSD1 were obtained from Protein Data Bank (PDB) (PDB code 2H94<sup>71</sup>). Two disordered loops with FASTA sequence EVKPPRDI and PSIPGAPQP were unresolved and thus built using MODELLER 9.10.<sup>74</sup> The protein was then protonated at pH 7.0 using MCCE 2.2.<sup>75,76</sup> The coordinates of the ligands **26** were obtained from their SMILES using OEChem TK (OpenEye Scientific Software). AM1-BCC charges were assigned as the partial charges of the ligands using Antechamber.<sup>77,78</sup>

Multiple conformers of ligand were generated using OMEGA (OpenEye Scientific Software) and docked into the FAD-binding site of LSD1 using OEDocking (OpenEye Scientific Software), which uses an exhaustive search algorithm and Chemgauss3 scoring function.<sup>79</sup> One-thousand binding poses were generated and clustered using a root mean square deviation (rmsd) metric to obtain the 10 most dissimilar clusters. Molecular dynamics (MD) simulations were subsequently performed on the centroid structures for each of the 10 clusters using GROMACS 4.6.2.<sup>80</sup> The amber99sb-ildn and GAFF force fields were used for the protein and ligands, respectively.<sup>81,82</sup> The protein–ligand complex was solvated in TIP3P water molecules. A 1500-step energy minimization and a 50 ps NVT equilibration simulation were performed at 300 K before a 1 ns production run was performed in the NPT ensemble using a time step of 2 fs. Snapshots were saved every 1 ps for analysis. The 10 1 ns production trajectories were concatenated for a Perron-cluster cluster analysis (PCCA),<sup>83</sup> which generated ~20 distinct structure clusters.

**SiRNA Transfection.** 6 × 10<sup>5</sup> cells were seeded in a six-well plate and then incubated for 3 days in standard medium in the presence of

20–100 nM siRNA directed against LSD1 or control siRNA (Scrambled) complexed with Lipofectamine RNAiMAX reagent according to the manufacturer's instructions.

**Migration and Invasion Assay.** For the wound healing assay, cells were plated in a 24-well plate, and the cell surface was scratched using a 10  $\mu$ L pipet tip. Then cells were treated with compound **26** with different concentrations followed by a 48 h incubation and photographed on an inverted microscope.

For invasion assays, cells were plated in Transwell 24-well plates coated with diluted Matrigel. In the upper chamber, medium was supplemented with 1% heat-inactivated FBS. In the lower chamber, 20% FBS was used as chemoattractant. Different concentrations of compound **26** were added in the chamber. After 48 h, medium was removed and the chambers were washed twice with PBS. Noninvading cells were removed from the upper surface of the membrane by scrubbing with cotton tipped swab, and the invading cells were fixed with methanol for 15 min. Then the chambers were stained with 0.1% crystal violet for 30 min. Six fields for each chamber were photographed on an inverted microscope, and invading cells were counted in each field.

For migration assays, cells were plated in Transwell 24-well plates without Matrigel. The medium, attractant, staining, and cell counting method were the same as those of the invasion assay.

**Immunoprecipitation and Western Blot.** Cross-linked immunoprecipitation was performed with the commercialized kit from Thermo Fisher. Western blot was performed with the total lysates by RIPA or histone purified with kit from Epigentek. Equal amounts of cell lysates were denatured, separated by SDS–PAGE, and transferred to 0.2  $\mu$ m nitrocellulose membranes. After blocking with PBS containing 5% nonfat dry milk, the membranes were incubated overnight at 4 °C with primary antibody, followed by incubation with a horseradish peroxidase-conjugated secondary antibody. The immunoblots were visualized by enhanced chemiluminescence kit from Thermo Fisher.

Antibodies used were against histone H3K4me (Selleck Chemicals no. A1237), H3K4me2 (Epitomics no. 1347-1), H3K9me2 (Epitomics no. 1349-1), H3K4me3 (Bioss, bs-4715R), total H3 (Sino Biological Inc. no. 100005-MM01), LSD1 (Epitomics no. 5890-1), E-cadherin (Epitomics no. 1702-1), Snail (Cell Signaling no. 3879), GAPDH (GoodHere no. AB-M-M 001).

**Apoptotic Analysis.** Changes in cell morphology were analyzed by Hoechst-33258 staining. Cells were treated with compound **26** at the indicated concentrations for 48 h. Then the cells were fixed and stained with 5  $\mu$ g/mL Hoechst-33258. After staining, the cells were washed. Apoptotic cells were examined and identified according to the condensation and fragmentation of their nuclei by fluorescence microscopy.

The apoptosis was quantified by FACS with annexinV-FITC/PI staining kit from Biovision. Ten-thousand events for each sample were counted and analyzed by Accuri C6 flow cytometer. The early and late apoptotic cells were identified by the localization of annexin V and PI.

**Xenograft Studies.** Xenograft models using human gastric cancer cell line (MGC-803) was established in BALB/C mice. Once the tumors reached 100 mm<sup>3</sup>, mice were divided into control groups (saline and hydroxypropyl- $\beta$ -cyclodextrin) and treatment groups. The treatment groups received compound **26** (5, 10, 20 mg/kg prepared with hydroxypropyl- $\beta$ -cyclodextrin) iv per day for a period of 21 days. Tumor volumes were measured at 3-day intervals. After the 21st day, the mice were euthanized and the tumors were isolated and weighed. Tumor size was determined by caliper measurements, and the body weight was measured at 3-day intervals to monitor drug toxicity.

**Statistical Analyses.** Data were expressed as the mean  $\pm$  SD. The significance of the difference between different groups was determined with analysis of variance (ANOVA) and Student *t* test. Results were considered statistically significant at *P* < 0.05. *P* < 0.01 was considered highly significant.

## ■ ASSOCIATED CONTENT

### § Supporting Information

Characterization data for selected compounds. This material is available free of charge via the Internet at <http://pubs.acs.org>.

## ■ AUTHOR INFORMATION

### Corresponding Author

\*Phone: +86-371-67781739. E-mail: [liuhm@zzu.edu.cn](mailto:liuhm@zzu.edu.cn).

### Author Contributions

\*Y.-C.Z. and Y.-C.D. contributed equally.

### Notes

The authors declare no competing financial interest.

## ■ ACKNOWLEDGMENTS

This work was supported by National Natural Science Foundation of China (Project No. 81172937 for H.-M.L. and Project No. 81270270 for W.Z.). We are grateful to Dr. Shaomin Wang, Analysis and Testing Center, Zhengzhou University, for performing the HR-ESI-MS experiments, and Bing Zhao, School of Pharmaceutical Sciences, Zhengzhou University, for the NMR analysis. We also thank Liang Zhou (Quantum Design China & NanoTemper Technologies GmbH) for providing the Microscale Thermophoresis (MST) assay.

## ■ ABBREVIATIONS USED

LSD1, histone lysine specific demethylase 1; LSD2, histone lysine specific demethylase 2; HKMT, histone lysine methyltransferase; HKDM, histone demethylase; DNMT, DNA methyltransferase; MAO, monoamine oxidase; HDAC, histone deacetylase; DSF, disulfiram; MRSA, methicillin-resistant *Staphylococcus aureus*; FAD, flavin adenine dinucleotide; 2-PCPA, tranlylcypromine; HPLC, high performance liquid chromatography; MST, microscale thermophoresis; HP- $\beta$ -CD, hydroxypropyl- $\beta$ -cyclodextrin; FBS, fetal bovine serum; SD, standard deviation

## ■ REFERENCES

- (1) Shi, Y.; Lan, F.; Matson, C.; Mulligan, P.; Whetstone, J. R.; Cole, P. A.; Casero, R. A. Histone demethylation mediated by the nuclear amine oxidase homolog LSD1. *Cell* **2004**, *119*, 941–953.
- (2) Wang, J.; Hevi, S.; Kurash, J. K.; Lei, H.; Gay, F.; Bajko, J.; Su, H.; Sun, W.; Chang, H.; Xu, G.; Gaudet, F.; Li, E.; Chen, T. The lysine demethylase LSD1 (KDM1) is required for maintenance of global DNA methylation. *Nat. Genet.* **2009**, *41*, 125–129.
- (3) Ooi, S. K.; Qiu, C.; Bernstein, E.; Li, K.; Jia, D.; Yang, Z.; Erdjument-Bromage, H.; Tempst, P.; Lin, S. P.; Allis, C. D.; Cheng, X.; Bestor, T. H. DNMT3L connects unmethylated lysine 4 of histone H3 to de novo methylation of DNA. *Nature* **2007**, *448*, 714–717.
- (4) Ciccone, D. N.; Su, H.; Hevi, S.; Gay, F.; Lei, H.; Bajko, J.; Xu, G.; Li, E.; Chen, T. KDM1B is a histone H3K4 demethylase required to establish maternal genomic imprints. *Nature* **2009**, *461*, 415–418.
- (5) Huang, J.; Sengupta, R.; Espejo, A. B.; Lee, M. G.; Dorsey, J. A.; Richter, M.; Opravil, S.; Shiekhata, R.; Bedford, M. T.; Jenuwein, T.; Berger, S. L. p53 is regulated by the lysine demethylase LSD1. *Nature* **2007**, *449*, 105–108.
- (6) Scoumanne, A.; Chen, X. The lysine-specific demethylase 1 is required for cell proliferation in both p53-dependent and -independent manners. *J. Biol. Chem.* **2007**, *282*, 15471–15475.
- (7) Kontaki, H.; Talianidis, I. Lysine methylation regulates E2F1-induced cell death. *Mol. Cell* **2010**, *39*, 152–160.
- (8) Metzger, E.; Wissmann, M.; Yin, N.; Muller, J. M.; Schneider, R.; Peters, A. H.; Gunther, T.; Buettner, R.; Schule, R. LSD1 demethylates



repressive histone marks to promote androgen-receptor-dependent transcription. *Nature* **2005**, *437*, 436–439.

(9) Cai, C.; He, H. H.; Chen, S.; Coleman, I.; Wang, H.; Fang, Z.; Nelson, P. S.; Liu, X. S.; Brown, M.; Balk, S. P. Androgen receptor gene expression in prostate cancer is directly suppressed by the androgen receptor through recruitment of lysine-specific demethylase 1. *Cancer Cell* **2011**, *20*, 457–471.

(10) Lim, S.; Janzer, A.; Becker, A.; Zimmer, A.; Schule, R.; Buettner, R.; Kirfel, J. Lysine-specific demethylase 1 (LSD1) is highly expressed in ER-negative breast cancers and a biomarker predicting aggressive biology. *Carcinogenesis* **2010**, *31*, 512–520.

(11) Pollock, J. A.; Larrea, M. D.; Jasper, J. S.; McDonnell, D. P.; McCafferty, D. G. Lysine-specific histone demethylase 1 inhibitors control breast cancer proliferation in ER $\alpha$ -dependent and -independent manners. *ACS Chem. Biol.* **2012**, *7*, 1221–1231.

(12) Zhu, Q.; Huang, Y.; Marton, L. J.; Woster, P. M.; Davidson, N. E.; Casero, R. A., Jr. Polyamine analogs modulate gene expression by inhibiting lysine-specific demethylase 1 (LSD1) and altering chromatin structure in human breast cancer cells. *Amino Acids* **2012**, *42*, 887–898.

(13) Magerl, C.; Ellinger, J.; Braunschweig, T.; Kremmer, E.; Koch, L. K.; Holler, T.; Buttner, R.; Luscher, B.; Gutgemann, I. H3K4 dimethylation in hepatocellular carcinoma is rare compared with other hepatobiliary and gastrointestinal carcinomas and correlates with expression of the methylase Ash2 and the demethylase LSD1. *Hum. Pathol.* **2010**, *41*, 181–189.

(14) Bennani-Baiti, I. M.; Machado, I.; Llombart-Bosch, A.; Kovar, H. Lysine-specific demethylase 1 (LSD1/KDM1A/AOF2/BHC110) is expressed and is an epigenetic drug target in chondrosarcoma, Ewing's sarcoma, osteosarcoma, and rhabdomyosarcoma. *Hum. Pathol.* **2012**, *43*, 1300–1307.

(15) Hayami, S.; Kelly, J. D.; Cho, H. S.; Yoshimatsu, M.; Unoki, M.; Tsunoda, T.; Field, H. I.; Neal, D. E.; Yamaue, H.; Ponder, B. A. Overexpression of LSD1 contributes to human carcinogenesis through chromatin regulation in various cancers. *Int. J. Cancer* **2011**, *128*, 574–586.

(16) Lv, T.; Yuan, D.; Miao, X.; Lv, Y.; Zhan, P.; Shen, X.; Song, Y. Over-expression of LSD1 promotes proliferation, migration and invasion in non-small cell lung cancer. *PLoS One* **2012**, *7*, e35065.

(17) Suzuki, T.; Miyata, N. Lysine demethylases inhibitors. *J. Med. Chem.* **2011**, *54*, 8236–8250.

(18) Huang, Y.; Greene, E.; Murray Stewart, T.; Goodwin, A. C.; Baylin, S. B.; Woster, P. M.; Casero, R. A., Jr. Inhibition of lysine-specific demethylase 1 by polyamine analogues results in reexpression of aberrantly silenced genes. *Proc. Natl. Acad. Sci. U.S.A.* **2007**, *104*, 8023–8028.

(19) Dulla, B.; Kirla, K. T.; Rathore, V.; Deora, G. S.; Kavela, S.; Maddika, S.; Chatti, K.; Reiser, O.; Iqbal, J.; Pal, M. Synthesis and evaluation of 3-amino/guanidine substituted phenyl oxazoles as a novel class of LSD1 inhibitors with anti-proliferative properties. *Org. Biomol. Chem.* **2013**, *11*, 3103–3107.

(20) Wu, Y.; Steinbergs, N.; Murray-Stewart, T.; Marton, L. J.; Casero, R. A. Oligoamine analogues in combination with 2-difluoromethylornithine synergistically induce re-expression of aberrantly silenced tumour-suppressor genes. *Biochem. J.* **2012**, *442*, 693–701.

(21) Willmann, D.; Lim, S.; Wetzel, S.; Metzger, E.; Jandausch, A.; Wilk, W.; Jung, M.; Forne, I.; Imhof, A.; Janzer, A.; Kirfel, J.; Waldmann, H.; Schule, R.; Buettner, R. Impairment of prostate cancer cell growth by a selective and reversible LSD1 inhibitor. *Int. J. Cancer* **2012**, *131*, 2704–2709.

(22) Hazeldine, S.; Pachaiyappan, B.; Steinbergs, N.; Nowotarski, S.; Hanson, A. S.; Casero, R. A., Jr.; Woster, P. M. Low molecular weight amidoximes that act as potent inhibitors of lysine-specific demethylase 1. *J. Med. Chem.* **2012**, *55*, 7378–7391.

(23) Lohse, B.; Kristensen, J. L.; Kristensen, L. H.; Agger, K.; Helin, K.; Gajhede, M.; Clausen, R. P. Inhibitors of histone demethylases. *Bioorg. Med. Chem.* **2011**, *19*, 3625–2636.

(24) Edmondson, D. E.; Mattevi, A.; Binda, C.; Li, M.; Hubalek, F. Structure and mechanism of monoamine oxidase. *Curr. Med. Chem.* **2004**, *11*, 1983–1993.

(25) Lee, M. G.; Wynder, C.; Schmidt, D. M.; McCafferty, D. G.; Shiekhhattar, R. Histone H3 lysine 4 demethylation is a target of nonselective antidepressive medications. *Chem. Biol.* **2006**, *13*, 563–567.

(26) Culhane, J. C.; Szewczuk, L. M.; Liu, X.; Da, G.; Marmorstein, R.; Cole, P. A. A mechanism-based inactivator for histone demethylase LSD1. *J. Am. Chem. Soc.* **2006**, *128*, 4536–4537.

(27) Huang, Y.; Stewart, T. M.; Wu, Y.; Baylin, S. B.; Marton, L. J.; Perkins, B.; Jones, R. J.; Woster, P. M.; Casero, R. A., Jr. Novel oligoamine analogues inhibit lysine-specific demethylase 1 and induce reexpression of epigenetically silenced genes. *Clin. Cancer Res.* **2009**, *15*, 7217–7128.

(28) Ueda, R.; Suzuki, T.; Mino, K.; Tsumoto, H.; Nakagawa, H.; Hasegawa, M.; Sasaki, R.; Mizukami, T.; Miyata, N. Identification of cell-active lysine specific demethylase 1-selective inhibitors. *J. Am. Chem. Soc.* **2009**, *131*, 17536–17537.

(29) Sharma, S. K.; Wu, Y.; Steinbergs, N.; Crowley, M. L.; Hanson, A. S.; Casero, R. A.; Woster, P. M. (Bis)urea and (bis)thiourea inhibitors of lysine-specific demethylase 1 as epigenetic modulators. *J. Med. Chem.* **2010**, *53*, 5197–5212.

(30) Mimasu, S.; Umezawa, N.; Sato, S.; Higuchi, T.; Umehara, T.; Yokoyama, S. Structurally designed trans-2-phenylcyclopropylamine derivatives potentially inhibit histone demethylase LSD1/KDM1. *Biochemistry* **2010**, *49*, 6494–6503.

(31) Binda, C.; Valente, S.; Romanenghi, M.; Pilotto, S.; Cirilli, R.; Karytinis, A.; Ciossani, G.; Botrugno, O. A.; Forneris, F.; Tardugno, M.; Edmondson, D. E.; Minucci, S.; Mattevi, A.; Mai, A. Biochemical, structural, and biological evaluation of tranylcypromine derivatives as inhibitors of histone demethylases LSD1 and LSD2. *J. Am. Chem. Soc.* **2010**, *132*, 6827–6833.

(32) Culhane, J. C.; Wang, D.; Yen, P. M.; Cole, P. A. Comparative analysis of small molecules and histone substrate analogues as LSD1 lysine demethylase inhibitors. *J. Am. Chem. Soc.* **2010**, *132*, 3164–3176.

(33) Tortorici, M.; Borrello, M. T.; Tardugno, M.; Chiarelli, L. R.; Pilotto, S.; Ciossani, G.; Vellore, N. A.; Bailey, S. G.; Cowan, J.; O'Connell, M.; Crabb, S. J.; Packham, G.; Mai, A.; Baron, R.; Ganesan, A.; Mattevi, A. Protein recognition by short peptide reversible inhibitors of the chromatin-modifying LSD1/CoREST lysine demethylase. *ACS Chem. Biol.* **2013**, *8*, 1677–1682.

(34) Wang, J.; Lu, F.; Ren, Q.; Sun, H.; Xu, Z.; Lan, R.; Liu, Y.; Ward, D.; Quan, J.; Ye, T.; Zhang, H. Novel histone demethylase LSD1 inhibitors selectively target cancer cells with pluripotent stem cell properties. *Cancer Res.* **2011**, *71*, 7238–7249.

(35) Zifcsak, C. A.; Hlasta, D. J. Current methods for the synthesis of 2-substituted azoles. *Tetrahedron* **2004**, *60*, 8991–9016.

(36) Davies, J. R.; Kane, P. D.; Moody, C. J. N–H insertion reactions of rhodium carbenoids. Part 5: A convenient route to 1,3-azoles. *Tetrahedron* **2004**, *60*, 3967–3977.

(37) Chimenti, F.; Maccioni, E.; Secci, D.; Bolasco, A.; Chimenti, P.; Granese, A.; Carradori, S.; Alcaro, S.; Ortuso, F.; Yanez, M.; Orallo, F.; Cirilli, R.; Ferretti, R.; La Torre, F. Synthesis, stereochemical identification, and selective inhibitory activity against human monoamine oxidase-B of 2-methylcyclohexylidene-(4-arylthiazol-2-yl)-hydrazones. *J. Med. Chem.* **2008**, *51*, 4874–4880.

(38) Chimenti, F.; Fioravanti, R.; Bolasco, A.; Manna, F.; Chimenti, P.; Secci, D.; Befani, O.; Turini, P.; Ortuso, F.; Alcaro, S. Monoamine oxidase isoform-dependent tautomeric influence in the recognition of 3,5-diaryl pyrazole inhibitors. *J. Med. Chem.* **2007**, *50*, 425–428.

(39) La Regina, G.; Silvestri, R.; Artico, M.; Lavecchia, A.; Novellino, E.; Befani, O.; Turini, P.; Agostinelli, E. New pyrrole inhibitors of monoamine oxidase: synthesis, biological evaluation, and structural determinants of MAO-A and MAO-B selectivity. *J. Med. Chem.* **2007**, *50*, 922–931.

(40) Valente, S.; Tomassi, S.; Tempera, G.; Saccoccio, S.; Agostinelli, E.; Mai, A. Novel reversible monoamine oxidase A inhibitors: highly

potent and selective 3-(1H-pyrrol-3-yl)-2-oxazolidinones. *J. Med. Chem.* **2011**, *54*, 8228–8232.

(41) Maccioni, E.; Alcaro, S.; Cirilli, R.; Vigo, S.; Cardia, M. C.; Sanna, M. L.; Meleddu, R.; Yanez, M.; Costa, G.; Casu, L.; Matyus, P.; Distinto, S. 3-Acetyl-2,5-diaryl-2,3-dihydro-1,3,4-oxadiazoles: a new scaffold for the selective inhibition of monoamine oxidase B. *J. Med. Chem.* **2011**, *54*, 6394–6398.

(42) Gentili, F.; Pizzinat, N.; Ordener, C.; Marchal-Victorion, S.; Maurel, A.; Hofmann, R.; Renard, P.; Delagrè, P.; Pignini, M.; Parini, A.; Giannella, M. 3-[5-(4,5-Dihydro-1H-imidazol-2-yl)-furan-2-yl]-phenylamine (amifuraline), a promising reversible and selective peripheral MAO-A inhibitor. *J. Med. Chem.* **2006**, *49*, 5578–5586.

(43) Chimenti, F.; Maccioni, E.; Secci, D.; Bolasco, A.; Chimenti, P.; Granese, A.; Befani, O.; Turini, P.; Alcaro, S.; Ortuso, F.; Cirilli, R.; La Torre, F.; Cardia, M. C.; Distinto, S. Synthesis, molecular modeling studies, and selective inhibitory activity against monoamine oxidase of 1-thiocarbamoyl-3,5-diaryl-4,5-dihydro-(1H)-pyrazole derivatives. *J. Med. Chem.* **2005**, *48*, 7113–7122.

(44) Jia, Z.; Zhu, Q. “Click” assembly of selective inhibitors for MAO-A. *Bioorg. Med. Chem. Lett.* **2010**, *20*, 6222–6225.

(45) Reck, F.; Zhou, F.; Girardot, M.; Kern, G.; Eyermann, C. J.; Hales, N. J.; Ramsay, R. R.; Gravestock, M. B. Identification of 4-substituted 1,2,3-triazoles as novel oxazolidinone antibacterial agents with reduced activity against monoamine oxidase A. *J. Med. Chem.* **2005**, *48*, 499–506.

(46) Suzuki, T.; Ota, Y.; Ri, M.; Bando, M.; Gotoh, A.; Ito, Y.; Tsumoto, H.; Tatum, P. R.; Mizukami, T.; Nakagawa, H.; Iida, S.; Ueda, R.; Shirahige, K.; Miyata, N. Rapid discovery of highly potent and selective inhibitors of histone deacetylase 8 using click chemistry to generate candidate libraries. *J. Med. Chem.* **2012**, *55*, 9562–9575.

(47) Hou, J.; Li, Z.; Fang, Q.; Feng, C.; Zhang, H.; Guo, W.; Wang, H.; Gu, G.; Tian, Y.; Liu, P.; Liu, R.; Lin, J.; Shi, Y.-k.; Yin, Z.; Shen, J.; Wang, P. G. Discovery and extensive in vitro evaluations of NK-HDAC-1: a chiral histone deacetylase inhibitor as a promising lead. *J. Med. Chem.* **2012**, *55*, 3066–3075.

(48) Imamura, H.; Ohtake, N.; Jona, H.; Shimizu, A.; Moriya, M.; Sato, H.; Sugimoto, Y.; Ikeura, C.; Kiyonaga, H.; Nakano, M.; Nagano, R.; Abe, S.; Yamada, K.; Hashizume, T.; Morishima, H. Dicationic dithiocarbamate carbapenems with anti-MRSA activity. *Bioorg. Med. Chem.* **2001**, *9*, 1571–1578.

(49) Ronconi, L.; Marzano, C.; Zanello, P.; Corsini, M.; Miolo, G.; Maccà, C.; Trevisan, A.; Fregona, D. Gold(III) dithiocarbamate derivatives for the treatment of cancer: solution chemistry, DNA binding, and hemolytic properties. *J. Med. Chem.* **2006**, *49*, 1648–1657.

(50) Len, C.; Boulogne-Merlot, A.-S.; Postel, D.; Ronco, G.; Villa, P.; Goubert, C.; Jeufraut, E.; Mathon, B.; Simon, H. Synthesis and antifungal activity of novel bis(dithiocarbamate) derivatives of glycerol. *J. Agric. Food Chem.* **1996**, *44*, 2856–2858.

(51) Cvek, B.; Dvorak, Z. Targeting of nuclear factor-kappaB and proteasome by dithiocarbamate complexes with metals. *Curr. Pharm. Des.* **2007**, *13*, 3155–3167.

(52) Adachi, Y.; Nakamura, K.; Kato, Y.; Hazumi, N.; Hashizume, T.; Nakagawa, S. In vitro evaluation of BO-3482, a novel dithiocarbamate carbapenem with activity against methicillin-resistant staphylococci. *Antimicrob. Agents Chemother.* **1997**, *41*, 2282–2285.

(53) Nagano, R.; Shibata, K.; Naito, T.; Fuse, A.; Asano, K.; Hashizume, T.; Nakagawa, S. Therapeutic efficacy of BO-3482, a novel dithiocarbamate carbapenem, in mice infected with methicillin-resistant *Staphylococcus aureus*. *Antimicrob. Agents Chemother.* **1997**, *41*, 2278–2281.

(54) Wang, X.-J.; Xu, H.-W.; Guo, L.-L.; Zheng, J.-X.; Xu, B.; Guo, X.; Zheng, C.-X.; Liu, H.-M. Synthesis and in vitro antitumor activity of new butenolide-containing dithiocarbamates. *Bioorg. Med. Chem. Lett.* **2011**, *21*, 3074–3077.

(55) Duan, Y.-C.; Ma, Y.-C.; Zhang, E.; Shi, X.-J.; Wang, M.-M.; Ye, X.-W.; Liu, H.-M. Design and synthesis of novel 1,2,3-triazole-dithiocarbamate hybrids as potential anticancer agents. *Eur. J. Med. Chem.* **2013**, *62*, 11–19.

(56) Hu, M.; Li, J.; Q. Yao, S. In situ “click” assembly of small molecule matrix metalloprotease inhibitors containing zinc-chelating groups. *Org. Lett.* **2008**, *10*, 5529–5531.

(57) Boeckman, R. K.; Ko, S. S. Stereochemical control in the intramolecular Diels–Alder reaction. 2. Structural and electronic effects on reactivity and selectivity. *J. Am. Chem. Soc.* **1982**, *104*, 1033–1041.

(58) Wang, E. S.; Choy, Y. M.; Wong, H. N. C. Synthetic studies on prehispanolone and 14,15-dihydroprehispanolone. *Tetrahedron* **1996**, *52*, 12137–12158.

(59) Lineweaver, H.; Burk, D. The determination of enzyme dissociation constants. *J. Am. Chem. Soc.* **1934**, *56*, 658–666.

(60) Burton, K. The stabilization of D-amino acid oxidase by flavin-adenine dinucleotide, substrates and competitive inhibitors. *Biochem. J.* **1951**, *48*, 458–467.

(61) Caldinelli, L.; Molla, G.; Bracci, L.; Lelli, B.; Pileri, S.; Cappelletti, P.; Sacchi, S.; Pollegioni, L. Effect of ligand binding on human D-amino acid oxidase: implications for the development of new drugs for schizophrenia treatment. *Protein Sci.* **2010**, *19*, 1500–1512.

(62) Hirota, T.; Lee, J. W.; St; John, P. C.; Sawa, M.; Iwaisako, K.; Noguchi, T.; Pongsawakul, P. Y.; Sonntag, T.; Welsh, D. K.; Brenner, D. A.; Doyle, F. J., 3rd; Schultz, P. G.; Kay, S. A. Identification of small molecule activators of cryptochrome. *Science* **2012**, *337*, 1094–1097.

(63) Chu, Y.; Chen, X.; Yang, Y.; Tang, Y. Identification of small molecular inhibitors for Ero1p by structure-based virtual screening. *Bioorg. Med. Chem. Lett.* **2011**, *21*, 1118–1121.

(64) Blais, J. D.; Chin, K. T.; Zito, E.; Zhang, Y.; Heldman, N.; Harding, H. P.; Fass, D.; Thorpe, C.; Ron, D. A small molecule inhibitor of endoplasmic reticulum oxidation 1 (ERO1) with selectively reversible thiol reactivity. *J. Biol. Chem.* **2010**, *285*, 20993–21003.

(65) Stavropoulos, P.; Blobel, G.; Hoelz, A. Crystal structure and mechanism of human lysine-specific demethylase-1. *Nat. Struct. Mol. Biol.* **2006**, *13*, 626–632.

(66) Baron, R.; Vellore, N. A. LSD1/CoREST is an allosteric nanoscale clamp regulated by H3-histone-tail molecular recognition. *Proc. Natl. Acad. Sci. U.S.A.* **2012**, *109*, 12509–12514.

(67) Robertson, J. C.; Hurley, N. C.; Tortorici, M.; Ciozzani, G.; Borrello, M. T.; Vellore, N. A.; Ganesan, A.; Mattevi, A.; Baron, R. Expanding the druggable space of the LSD1/CoREST epigenetic target: new potential binding regions for drug-like molecules, peptides, protein partners, and chromatin. *PLoS Comput. Biol.* **2013**, *9*, e1003158.

(68) Karytinis, A.; Forneris, F.; Profumo, A.; Ciozzani, G.; Battaglioli, E.; Binda, C.; Mattevi, A. A novel mammalian flavin-dependent histone demethylase. *J. Biol. Chem.* **2009**, *284*, 17775–17782.

(69) Zhang, Q.; Qi, S.; Xu, M.; Yu, L.; Tao, Y.; Deng, Z.; Wu, W.; Li, J.; Chen, Z.; Wong, J. Structure–function analysis reveals a novel mechanism for regulation of histone demethylase LSD2/AOF1/KDM1b. *Cell Res.* **2013**, *23*, 225–241.

(70) Karasulu, B.; Patil, M.; Thiel, W. Amine oxidation mediated by lysine-specific demethylase 1: quantum mechanics/molecular mechanics insights into mechanism and role of lysine 661. *J. Am. Chem. Soc.* **2013**, *135*, 13400–13413.

(71) Chen, Y.; Yang, Y.; Wang, F.; Wan, K.; Yamane, K.; Zhang, Y.; Lei, M. Crystal structure of human histone lysine-specific demethylase 1 (LSD1). *Proc. Natl. Acad. Sci. U.S.A.* **2006**, *103*, 13956–13961.

(72) Ferrari-Amorotti, G.; Fragiasso, V.; Esteki, R.; Prudente, Z.; Soliera, A. R.; Cattelan, S.; Manzotti, G.; Grisendi, G.; Dominici, M.; Pieracciolli, M.; Raschella, G.; Chiodoni, C.; Colombo, M. P.; Calabretta, B. Inhibiting interactions of lysine demethylase LSD1 with snail/slug blocks cancer cell invasion. *Cancer Res.* **2013**, *73*, 235–245.

(73) Zhou, M.; Diwu, Z.; Panchuk-Voloshina, N.; Haugland, R. P. A stable nonfluorescent derivative of resorufin for the fluorometric determination of trace hydrogen peroxide: applications in detecting the activity of phagocyte NADPH oxidase and other oxidases. *Anal. Biochem.* **1997**, *253*, 162–168.



- (74) Marti-Renom, M. A.; Stuart, A. C.; Fiser, A.; Sanchez, R.; Melo, F.; Sali, A. Comparative protein structure modeling of genes and genomes. *Annu. Rev. Biophys. Biomol. Struct.* **2000**, *29*, 291–325.
- (75) Georgescu, R. E.; Alexov, E. G.; Gunner, M. R. Combining conformational flexibility and continuum electrostatics for calculating pK(a)s in proteins. *Biophys. J.* **2002**, *83*, 1731–1748.
- (76) Alexov, E. G.; Gunner, M. R. Incorporating protein conformational flexibility into the calculation of pH-dependent protein properties. *Biophys. J.* **1997**, *72*, 2075–2093.
- (77) Jakalian, A.; Jack, D. B.; Bayly, C. I. Fast, efficient generation of high-quality atomic charges. AM1-BCC model: II. Parameterization and validation. *J. Comput. Chem.* **2002**, *23*, 1623–1641.
- (78) Wang, J.; Wang, W.; Kollman, P. A.; Case, D. A. Automatic atom type and bond type perception in molecular mechanical calculations. *J. Mol. Graphics Modell.* **2006**, *25*, 247–260.
- (79) McGann, M. FRED pose prediction and virtual screening accuracy. *J. Chem. Inf. Model.* **2011**, *51*, 578–596.
- (80) Hess, B.; Kutzner, C.; van der Spoel, D.; Lindahl, E. GROMACS 4: algorithms for highly efficient, load-balanced, and scalable molecular simulation. *J. Chem. Theory Comput.* **2008**, *4*, 435–447.
- (81) Lindorff-Larsen, K.; Piana, S.; Palmo, K.; Maragakis, P.; Klepeis, J. L.; Dror, R. O.; Shaw, D. E. Improved side-chain torsion potentials for the Amber ff99SB protein force field. *Proteins: Struct., Funct., Bioinf.* **2010**, *78*, 1950–1958.
- (82) Wang, J.; Wolf, R. M.; Caldwell, J. W.; Kollman, P. A.; Case, D. A. Development and testing of a general amber force field. *J. Comput. Chem.* **2004**, *25*, 1157–1174.
- (83) Deuffhard, P.; Huisinga, W.; Fischer, A.; Schütte, C. Identification of almost invariant aggregates in reversible nearly uncoupled Markov chains. *Linear Algebra Appl.* **2000**, *315*, 39–59.